# Electronic properties, correlated topology, and Green's function zeros

Chandan Setty,[1,2,*] Fang Xie,[1,†] Shouvik Sur,[1] Lei Chen,[1] Maia G. Vergniory,[3,4] and Qimiao Si[1]
[1]*Department of Physics and Astronomy, Rice Center for Quantum Materials, Rice University, Houston, Texas 77005, USA*
[2]*Department of Physics and Astronomy, Iowa State University, Ames, Iowa 50011, USA and Ames National Laboratory, U.S. Department of Energy, Ames, Iowa 50011, USA*
[3]*Donostia International Physics Center, P. Manuel de Lardizabal 4, 20018 Donostia-San Sebastian, Spain*
[4]*Max Planck Institute for Chemical Physics of Solids, Noethnitzer Strasse 40, 01187 Dresden, Germany*

(Received 28 September 2023; accepted 8 August 2024; published 3 September 2024)

There is extensive current interest in electronic topology in correlated settings. In strongly correlated systems, contours of Green's function zeros may develop in frequency-momentum space, and their role in correlated topology has increasingly been recognized. However, whether and how the zeros contribute to electronic properties is a matter of uncertainty. Here we address the issue in an exactly solvable model for a Mott insulator. We show that the Green's function zeros contribute to several physically measurable correlation functions in a way that does not run into inconsistencies. In particular, the physical properties remain robust to chemical potential variations up to the Mott gap, as it should be based on general considerations. Our work sets the stage for further understandings of the rich interplay among topology, symmetry, and strong correlations.

DOI: 10.1103/PhysRevResearch.6.033235

## I. INTRODUCTION

In noninteracting systems, electronic topology is formulated within band theory. Recent years have seen systematic development on how symmetries of crystalline lattices constrain topology and how they can be utilized to search for new topological materials [1–7]. In interacting settings, symmetry constraints have been considered in terms of Green's functions, either through a renormalized particle picture [8–10] in the form of a topological Hamiltonian [11,12] or by recognizing that the eigenvectors of the exact Green's function in a many-body system form a representation of a lattice space group [13]. The latter approach, which was introduced in the context of Weyl-Kondo semimetal [14–17] and provided the theoretical basis for its robustness [18], has led to the realization [19] that Green's function zeros [20] of an interacting lattice system obey symmetry constraints; accordingly, the Green's function zeros participate in the formation of correlated electronic topology, just as Green's function poles do. Concurrently, the role of Green's function zeros has been studied in the context of the edge spectrum of interacting topological insulators [21].

Quasiparticles represent the low-energy excitations of a Fermi liquid. The quasiparticles are conveniently described in terms of a Green's function approach in which they appear as poles of the single-particle Green's function [22]. They are characterized by the quasiparticle weight—a quantity that plays a central role in the microscopic Fermi liquid theory. When electron correlations are strong, the quasiparticle weight becomes very small, and its effect on observables is well documented; exemplary settings can be found in Refs. [23–26]. In the extreme correlation limit, the quasiparticle weight may vanish leading to a breakdown of the Fermi liquid. The precise manner in which thermodynamic and transport properties are affected by interactions in this limit is a central question in the field of correlation physics.

Mott insulators (MIs) occupy a special place in the physics of strongly correlated systems [27]. In MIs, the quasiparticle weight as well as the single-particle Green's function vanish to yield Green's function zeros along certain frequency-momentum contours. There has been considerable debate regarding the role of zeros on the physical charge and correlation functions [20,22,28–40].

Like poles across a Fermi surface, the real part of the Green's function changes sign across a zero surface, hence they contribute to the Luttinger volume [20,22] and single-particle winding numbers [33]. Similarly, zeros are key to the generalization of index theorems [28] to interacting settings, and they play an essential role in understanding symmetric mass generation [37,41–43]. In interacting topological insulators, it was argued that zeros allow for topological transitions to occur without closing the boundary gap [30,31,44].

While these properties raise the prospect of the zeros being experimentally measurable, their relationship to observables has been tenuous at best. For example, it is required that physical properties are independent of chemical potential variations up to the Mott scale at zero temperature [29] despite zeros occurring in the insulating gap. In addition, when determining the zeros' contribution to physically measurable correlations, it is crucial to keep track of conservation laws and the associated Ward identities. It is important to address these issues in order to properly assess the contributions of Green's function

*Contact author: csetty@rice.edu
†Contact author: fx7@rice.edu

zeros to physical properties. Furthermore, Green's function zeros are also difficult to probe experimentally. By definition, the vanishing spectral weight makes their detection challenging. Sharpening the theoretical understanding of how the Green's function zeros affect physical correlation functions is expected to be important for probing the zeros experimentally in the future.

In this work, we argue that certain robust physical properties of electron systems can indeed capture the contributions of the Green's function zeros, and, importantly, they do so in a way that is consistent with the aforementioned expectations. These properties can be exploited to indirectly gather properties that may otherwise be elusive to conventional probes. Our focus here is to illustrate how zeros *contribute* to observables in a consistent, gauge-invariant manner, rather than propose a concrete experimental setup in which they can be systematically extracted. We demonstrate our claims by considering an exactly solvable model of a MI [45] as a prototypical example where extreme correlation effects are realized [27].

More specifically, we compute here the charge and current response functions in accordance with the Ward identities, and we demonstrate how zeros manifest in physical observables. We begin by describing the exactly solvable models of interest in Sec. II [see Eqs. (1)–(4)]. In Sec. III, we reexamine the relationship between the Luttinger volume and self-energy in generic interacting settings. Using this relation, we provide a simple picture that elucidates how zeros are needed to preserve charge conservation while maintaining robustness of the total charge to changes in the chemical potential of the order of the Mott gap (see Figs. 1 and 2). More specifically, the total charge contains a term associated with the Luttinger volume and a "backflow" term [see Eq. (7)]. We use our procedure of considering the total charge as a guide to analyze other more involved physical quantities, with a focus on the topological Hall response. In this way, in Sec. IV we evaluate the Hall response for a MI starting from noninteracting Chern bands, and we show that it likewise contains two contributions [see Eqs. (35)–(37)]. The first is a quantized topological term proportional to the three-dimensional winding number $N_3$ [46,47] with contributions from Green's function zeros (see Fig. 4). The second is a previously unrecognized nonquantized backflow term essential to preserving charge conservation. In each case, the two terms combine to ensure that the total quantity is independent of changes to the chemical potential within the Mott gap *despite* containing contributions from zeros. We discuss some implications and conclude in Sec. V.

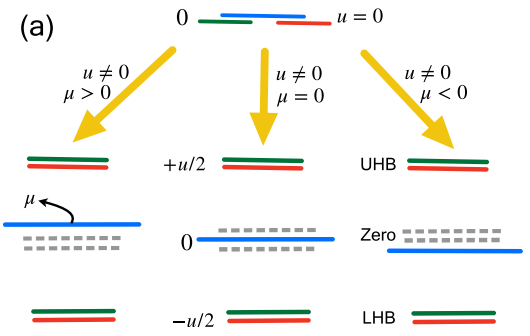


(b)

$N = v_l - \delta v$

| $\mu > 0$ | $G_0(z)$ | $G(z)$ | $R(z)$ | $\mu = 0$ | $G_0(z)$ | $G(z)$ | $R(z)$ | $\mu < 0$ | $G_0(z)$ | $G(z)$ | $R(z)$ |
|---|---|---|---|---|---|---|---|---|---|---|---|
| $n_<$ | 0-0 | 2-2 | 0 | $n_<$ | 0-0 | 2-0 | 2 | $n_<$ | 0-0 | 2-0 | 2 |
| $n_0$ | 2-0 | 0-0 | -2 | $n_0$ | 2-0 | 0-2 | -4 | $n_0$ | 2-0 | 0-0 | -2 |
| # | $N = 1$ | $v_l = 0$ | $\delta v = -1$ | # | $N = 1$ | $v_l = 1$ | $\delta v = 0$ | # | $N = 1$ | $v_l = 2$ | $\delta v = 1$ |

FIG. 1. Illustration of the Green's function zeros' contribution to the total particle count and the failure of pole counting. (a) Splitting of two occupied electronic states (red and green denote spin) at the Fermi energy into upper and lower Hubbard bands (UHB and LHB, respectively) due to the repulsive Coulomb interaction $u$ for the cases of $\mu > 0$, $\mu = 0$, and $\mu < 0$ in the atomic limit of the Hubbard model. The blue (dashed) line denotes the chemical potential (Green's function zeros). The vertical axis is frequency. (b) Tables showing the difference between the numbers of poles and zeros (# of poles − # of zeros) for the three cases of $\mu > 0$, $\mu = 0$, and $\mu < 0$. The rows $n_<(f)$, $n_0(f)$ label (# of poles − # of zeros) below and at the chemical potential, respectively, of the matrix $f$. "#" in the third row denotes the total contribution to the formula $N = v_l - \delta v$ in Eq. (7) using Eqs. (16), (11), and (15). The first two columns label the cases of noninteracting and interacting Green's function, respectively, and the third denotes the ratio of their determinants $R(z)$ [see Eq. (12)]. In each of the three cases, $N = v_l - \delta v$ is satisfied and the particle number is conserved despite variations of the Luttinger volume $v_l$ and its backflow deviation $\delta v$.

## II. MODEL

As an exactly solvable model in which Green's function zeros occur, we consider a generic multiband version of the Hatsugai-Kohmoto (HK) model [45]. We write the total Hamiltonian as

$$H = H_0 + H_I, \tag{1}$$

$$H_0 = \sum_{\boldsymbol{k},\alpha\sigma,\beta\sigma'} h_{\alpha\sigma,\beta\sigma'}(\boldsymbol{k}) c^\dagger_{\boldsymbol{k}\alpha\sigma} c_{\boldsymbol{k}\beta\sigma'}, \tag{2}$$

$$H_I = \frac{U}{2} \sum_{\boldsymbol{k}\alpha} (n_{\boldsymbol{k}\alpha\uparrow} + n_{\boldsymbol{k}\alpha\downarrow} - 1)^2 . \tag{3}$$

Here $c^\dagger_{\boldsymbol{k}\alpha\sigma}$ is the electron creation operator at momentum $\boldsymbol{k}$, orbital $\alpha$, and spin $\sigma$. The hopping matrix elements between states with orbital indices $\alpha, \beta$ and spin indices $\sigma, \sigma'$ are denoted by $h_{\alpha\sigma,\beta\sigma'}(\boldsymbol{k})$, $U$ is a four-fermion electron-electron interaction that is local in momentum space but highly nonlocal in real space, and $n_{\boldsymbol{k}\alpha\sigma}$ is the number operator. The Hamiltonian at each $\boldsymbol{k}$ point becomes mutually decoupled in the form $H = \sum_{\boldsymbol{k}} H_{\boldsymbol{k}}$, because of the local-in-momentum-space interaction. Later in the paper, we will also use a single-band version of Eq. (1) by replacing the kinetic hopping matrix by a single dispersion $\xi(\boldsymbol{k}) = \epsilon(\boldsymbol{k}) - \mu$, where $\epsilon(\boldsymbol{k})$ is the band energy and $\mu$ is the chemical potential. The interaction Hamiltonian then contains a single repulsive term between opposite spins at a specific momentum point. Accordingly, the orbital indices $\alpha, \beta$ are suppressed in the

electron creation and annihilation operators in Eq. (1) for the one-band model. We will explicitly specify when this is the case. The electronic and spectral properties of the Hamiltonian Eq. (1) for single- [19,34–36,45,48] and multiband dispersions [19,40,49] have been previously studied, but we recall some key properties. First, irrespective of the specific tight-binding Hamiltonian at hand, Eq. (1) captures a correlated metal to a fully gapped Mott insulator transition for interaction strength $U$ comparable to or larger than the noninteracting bandwidth ($W$). Second, the Green's function can be obtained exactly, and in the limit of strong interactions compared to $W$ and zero temperature, a key property of the Green's function is the existence of contours of dispersive zeros in the Mott gap. These contours are a consequence of destructive cancellation of electron addition- and removal-like transitions with equal and opposite energy transfers [19]. Further, lattice symmetries of the Hamiltonian $H$ constrain spectral degeneracies at high symmetry points that operate on both poles and zeros of the Green's function. Hence, Eq. (1) offers a platform to explore topological properties in the presence of interactions nonperturbatively even when there is a loss of quasiparticles. Additional properties of $H$ for the case when the noninteracting bands have a nontrivial spin-Hall Chern number are discussed in Ref. [19]. Due to these features, we use Eq. (1) as a starting point for our analysis.

In Sec. III and Fig. 2, it will suffice for us to work with a single-band version of Eq. (1). We will use a quadratic band dispersion of the form $\xi(\boldsymbol{k}) = k^2 - \mu$, where we denote $k$ as the magnitude of $\boldsymbol{k}$. In Sec. IV, we will work with a multiorbital tight-binding model with Chern bands to compute the conductivity. In this case, the matrix elements $h_{\alpha\sigma,\beta\sigma'}(\boldsymbol{k})$ are defined later in Eq. (42).

In the course of our discussion, we will also use the atomic limit of the Hubbard model to illustrate common features of certain conclusions. To establish notation, let us denote $n_{i\sigma}$ as the number operator at real space site $i$ and spin $\sigma$, and $u$ as the on-site Coulomb interaction. In this limit, we write the Hubbard Hamiltonian as

$$H_u = u\sum_i n_{i\uparrow}n_{i\downarrow} - \mu\sum_{i\sigma} c^\dagger_{i\sigma}c_{i\sigma}, \tag{4}$$

where $\mu$ is the on-site chemical potential, and $c^\dagger_{i\sigma}$ is the electron creation operator at site $i$ and spin $\sigma$. In this limit, one obtains an atomic Mott insulator where the single-site Green's function acquires dispersionless zeros when the probe frequency equals negative of the chemical potential [27]. Thus certain aspects and properties of the Hamiltonian Eq. (1) can be benchmarked against the physics of the Hubbard model. We now examine how physical properties are affected by the presence of zeros in the Green's function in Eqs. (1) and (4).

## III. TOTAL CHARGE

Before we study the specific case of Eq. (1), we begin by expressing the total particle number in terms of Green's function singularities [33]. With knowledge of the interacting Green's function $G(z)$, the total particle number $N$ can be determined from the following equation [50,51]:

$$N = \frac{1}{\beta}\sum_{\omega_n}\mathrm{Tr}[G(i\omega_n)]e^{i\omega_n\eta} = \oint\frac{dz}{2\pi i}n_F(z)\mathrm{Tr}[G(z)], \tag{5}$$

where $\omega_n$ is the fermionic Matsubara frequency, $\beta$ is the inverse temperature, $\eta$ is an infinitesimally small positive number, $n_F(z)$ is the Fermi function, and the contour of integration encloses the Matsubara frequencies along the imaginary axis. To extract the topological winding characteristics of the particle number [33], we note that the total Green's function can be written in terms of the noninteracting Green's function $G_0(i\omega_n)$ and self-energy $\Sigma(i\omega_n)$ through the Dyson equation $G(i\omega_n)^{-1} = G_0(i\omega_n)^{-1} - \Sigma(i\omega_n)$. Using this, we can rewrite

$$G(z) = G(z)\frac{\partial G(z)^{-1}}{\partial z} + G(z)\frac{\partial\Sigma(z)}{\partial z}, \tag{6}$$

and as a result the particle number $N$ takes the form

$$\begin{aligned} N &= \oint\frac{dz}{2\pi i}n_F(z)\left[\frac{\partial\ln\det G(z)^{-1}}{\partial z} + \mathrm{Tr}\left(G(z)\frac{\partial\Sigma(z)}{\partial z}\right)\right]. \\ &\equiv v_l - \delta v. \end{aligned} \tag{7}$$

The first term in Eq. (7) denoted $v_l$ is traditionally defined as the Luttinger volume, and the second backflow term in Eq. (7) denoted $\delta v$ is its deviation from the total particle number. The Luttinger theorem states that $\lim_{\beta\to\infty} N = \lim_{\beta\to\infty} v_l$. The theorem holds when particle-hole symmetry is preserved, and we will see below that away from the particle-hole symmetric filling, the Luttinger theorem can be violated and the backflow term $\lim_{\beta\to\infty}\delta v \neq 0$. To further simplify Eq. (7), we utilize the analytical properties of the Green's function. In particular, we note that the determinant of the single-particle Green's function can be decomposed into products of poles and zeros [30],

$$\det G(z) = \frac{\prod_{i=1}^{n_Z}(z-\zeta_i)}{\prod_{i=1}^{n_P}(z-\pi_i)}, \tag{8}$$

where $\zeta_i$ ($n_Z$) and $\pi_i$ ($n_P$) are the locations (number) of zeros and poles of the Green's function determinant. Substituting the factorization into the Luttinger volume gives a finite-temperature expression

$$v_l = \sum_{i=1}^{n_P} n_F(\pi_i) - \sum_{i=1}^{n_Z} n_F(\zeta_i). \tag{9}$$

At zero temperature, each of the poles (zeros) below the Fermi energy contributes one (negative one) count to the Luttinger volume, while those at the Fermi energy contribute a $\frac{1}{2}$ ($-\frac{1}{2}$) count. Hence the Fermi function is reduced to the Heaviside step (Kronecker $\delta$) function for energies below (at) the Fermi energy, and we can rewrite the Luttinger volume as

$$\begin{aligned} v_l = &\left(\sum_i^{n_P}\Theta(-\pi_i) - \sum_i^{n_Z}\Theta(-\zeta_i)\right) \\ &+\frac{1}{2}\left(\sum_i^{n_P}\delta_{0,\pi_i} - \sum_i^{n_Z}\delta_{0,\zeta_i}\right). \end{aligned} \tag{10}$$

For notational simplicity and later discussions, we will denote the difference between the number of poles and zeros below

(at) the chemical potential for the determinant of the matrix $f$ as $n_<(f)$ $[n_0(f)]$. Thus the $v_l$ can be rewritten succinctly as

$$v_l = n_<(G) + \tfrac{1}{2} n_0(G). \tag{11}$$

Notice that in the scenario when there are no zeros in the Green's function, the Luttinger volume reduces to its well-known expression but with half the contribution from poles at the Fermi energy when compared to those below, as must be expected. We can similarly simplify the expression for the deviation from the Luttinger volume $\delta v$. Defining the ratio of the determinant of the noninteracting and interacting Green's function as

$$R(z) = \frac{\det G_0(z)}{\det G(z)}, \tag{12}$$

we can rewrite the deviation as an expression similar to the Luttinger volume but in terms of analytical properties of $R(z)$ [33]. Choosing a contour of integration that encloses the Matsubara frequencies along the imaginary axis, we have the backflow term [33]

$$\begin{aligned}\delta v &= -\oint \frac{dz}{2\pi i} n_F(z) \mathrm{Tr}\left( G(z) \frac{\partial \Sigma(z)}{\partial z} \right) \\ &= +\oint \frac{dz}{2\pi i} n_F(z) \frac{\partial \ln R(z)}{\partial z}. \end{aligned} \tag{13}$$

We now define $Z_i$ ($N_Z$) and $\Pi_i$ ($N_P$) as the locations (number) of zeros and poles of $R(z)$. We then obtain an expression for the backflow $\delta v$ similar to that of $v_l$ in Eq. (10) as

$$\begin{aligned}\delta v &= \left( \sum_i^{N_P} \Theta(-\Pi_i) - \sum_i^{N_Z} \Theta(-Z_i) \right) \\ &\quad + \frac{1}{2} \left( \sum_i^{N_P} \delta_{0,\Pi_i} - \sum_i^{N_Z} \delta_{0,Z_i} \right) \qquad (14) \\ &= n_<(R^{-1}) + \frac{1}{2} n_0(R^{-1}). \qquad (15) \end{aligned}$$

In noninteracting systems, $G_0(z) = G(z)$ and by definition $R(z) = 1$ leading to $\delta v = 0$. The total particle number is fixed by that of the noninteracting electron Green's function, and it takes the form

$$N = n_<(G_0) + \tfrac{1}{2} n_0(G_0). \tag{16}$$

In a Fermi liquid and related phases, due to the absence of Green's function zeros in its determinant, there exists a one-to-one mapping between the poles of $G_0(z)$ and $G(z)$. This is because the lack of zeros leaves the pole structure of the Green's function determinant intact. Hence the Luttinger theorem continues to be satisfied and $\delta v = 0$. We are now in a position to calculate the particle number for different cases of interest, including the Hamiltonians described in Eqs. (1) and (4).

### A. Insights from the atomic limit

#### 1. Failure of pole counting

To elucidate the role of quasiparticle loss on the particle number, we begin with the atomic limit of the Hubbard model in Eq. (4). We argue that in this limit, counting of poles is insufficient to capture the total particle count. This fact is already reflected in Eqs. (7), (10), and (15), but here we give a simplified picture to help demonstrate a key notion—Green's function zeros in the Mott gap contribute to the total particle number while also keeping it invariant under changes to the chemical potential up to the order of the gap. We argue that this holds true for any physically measurable property. Later in the paper, we will further reiterate this simple principle in the context of a topological Hall response in the Mott phase obtained from the Hamiltonian in Eq. (1).

We work with the Hubbard Hamiltonian by setting the kinetic energy and chemical potential to zero, i.e.,

$$H_u = u \sum_i n_{i\uparrow} n_{i\downarrow}, \tag{17}$$

where $i$ runs over the various sites of the lattice. In the absence of interactions, the determinant of the noninteracting Green's function per site is given by $\det G_0(z) = \frac{1}{z^2}$, where the quadratic power in the denominator is due to the spin degree of freedom. This leads to *two* poles located exactly at zero energy as displayed in Fig. 1(a) with a weight of one-half each. In the presence of interactions and particle-hole symmetry, the determinant of the interacting Green's function $G_u(z)$ per site is given by

$$\det G_u(z) = \left( \frac{4z}{4z^2 - u^2} \right)^2, \tag{18}$$

where again the overall quadratic power is from the spin degree of freedom. Due to the pole in the self-energy $\Sigma(z) = \frac{u^2}{4z}$, the interacting Green's function has *four* poles—*two* poles each above and below the chemical potential—and *two* zeros at the chemical potential. This is shown below the center arrow in Fig. 1(a). As a result, there is a doubling of the number of poles *below* the Fermi energy each with a weight of unity. Hence counting poles by themselves in the atomic limit of the Hubbard model cannot be sufficient to account for a fixed total particle number. A comparison of the determinants of $G_0(z)$ and $G_u(z)$ readily lays out the reason for the failure of pole counting—a singular self-energy (Green's function zero) changes the order of the Green's function pole structure. Thus, while accounting for singularities of the Green's function in the Hubbard model, it is essential to count zeros for the preservation of the total particle number [22].

#### 2. Role of zeros

From dimensionality arguments, the singularity of the self-energy must naturally be involved to account for the total Luttinger count and electron number. Equations (7), (10), and (15) precisely capture how Green's function zeros must be included to preserve the total particle number in the presence of interactions.

To better clarify the role of zeros, we compute the total particle number per site using Eqs. (7), (10), and (15) in the atomic limit of the Hubbard model [Eq. (4)]. We first work in the zero chemical potential limit and later consider scenarios in which it is nonzero. In the absence of interactions, we determine $v_l$ and $\delta v$ from the determinant of the noninteracting Green's function $\det G_0(z) = z^{-2}$. Since there are two poles at zero energy [Fig. 1(a)], $v_l = \frac{1}{2}(2) = 1$, whereas $\ln R(z) = 0$

leading to $\delta v = 0$; hence $N = v_l - \delta v = 1$ per site. In the presence of interactions, there are two poles below the Fermi energy and two zeros at the Fermi energy in the determinant Eq. (18) [Fig. 1(a)]. We therefore have $v_l = 2 - \frac{1}{2}(2) = 1$, whereas, since $R(z)^{-1} = \det G_u(z)/\det G_0(z) = \frac{4z^4}{(4z^2-u^2)^2}$, we have two poles below and four zeros at the Fermi energy giving $\delta v = 2 - \frac{1}{2}(4) = 0$; hence again $N = v_l - \delta v = 1$ per site. Thus we see that in the atomic limit of the Hubbard model, the Luttinger theorem holds when $\mu = 0$ (particle-hole symmetry), and to recover the correct particle number, Green's function zeros must contribute to the count.

Moving away from the $\mu = 0$ limit, we shift the chemical potential within the Mott gap away from the particle-hole symmetric point. For the case when $\mu < 0$ in the presence of interactions, there are two poles (no singularities) below (at) the chemical potential [Fig. 1(a)]. Hence we see that the Luttinger count is $v_l = 2 + \frac{1}{2}(0) = 2$, whereas the deviation is $\delta v = 2 + \frac{1}{2}(-2) = 1$, hence satisfying the same particle number condition $N = v_l - \delta v = 1$. Similarly when $\mu > 0$, there are two poles and zeros each (no singularities) below (at) the chemical potential [Fig. 1(a)]. We therefore have $v_l = 0 + \frac{1}{2}0 = 0$ and $\delta v = 0 + \frac{1}{2}(-2) = -1$ so that the particle number $N = v_l - \delta v = 1$ continues to remain unchanged. A summary of these numerical evaluations for the three cases of $\mu = 0, \mu > 0, \mu < 0$ appears in Fig. 1(b).

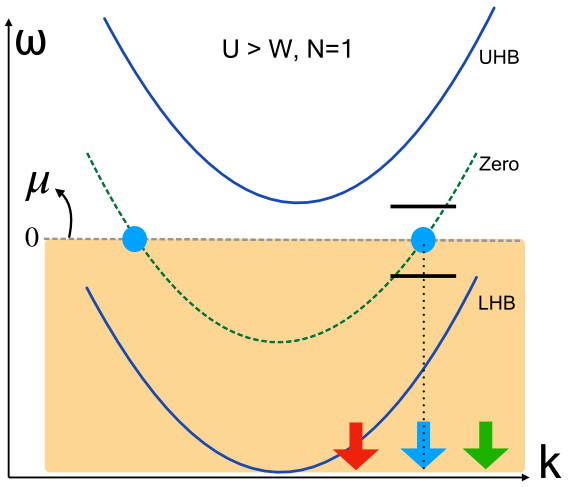


FIG. 2. Illustration of the upper Hubbard band (UHB), lower Hubbard band (LHB), and contour zero surface (dashed green line) of the model Hamiltonian in Eq. (1) with a single band. The blue dots denote the intersection of zero surface with the Fermi energy (horizontal dashed gray line). The red (green) arrow denotes a $\boldsymbol{k}$ point within (outside) the zero surface. The blue arrow denotes a $\boldsymbol{k}$ point at the zero surface. The short solid lines above and below the right blue dot denote the cases when the chemical potential is moved slightly above and below the reference value.

### B. The case of the Hatsugai-Kohmoto model

We can apply a similar analysis to the dispersive bands of the Hatsugai-Kohmoto model of Eq. (1). It is sufficient to consider a single-band version of the Hamiltonian to illustrate our results. Since the model is local in momentum space where the individual $\boldsymbol{k}$ points are decoupled from each other, every such momentum point can be viewed as a single-site Hubbard model with a different on-site energy. Hence the results from previous paragraphs for the single-site Hubbard model in the atomic limit can be utilized in a straightforward manner.

We focus on the limit where the interaction strength $U$ is larger than the bandwidth with an occupation $N = 1$ per spin (half-filling) and momentum point. Figure 2 shows a schematic of the spectral function in this limit. The solid lines are the upper and lower "Hubbard-like" bands, and the dashed line is the contour of Green's function zeros. The blue dots mark the intersection of the zero surface with the chemical potential, and the red (green) arrow denotes a momentum point inside (outside) the zero surface at zero energy [Luttinger surface (LS)]. At the particle hole symmetric point (solid blue dot), there exist two poles (two zeros) below (at) the chemical potential. Hence, like in the particle-hole symmetric case described earlier, we have $N = v_l = 1, \delta v = 0$. Away from particle-hole symmetry, the chemical potential can be moved above or below zero frequency (short black solid lines) for a given momentum corresponding to the blue arrow. Alternatively, the momenta can occur inside or outside the LS. For the case when the chemical potential is above zero, or equivalently when the momentum point lies inside the LS as marked by the red arrow, there are two poles and zeros below the chemical potential. As a result, $v_l = 0$ but $\delta v = -1$ so that the net particle count $N = 1$ continues to be preserved. Similarly, when the chemical potential is below zero, or equivalently when the momentum point lies outside the LS as marked by the green arrow, there are two poles below the chemical potential, and we obtain $v_l = 2$ but $\delta v = 1$ so that the net particle count is again $N = 1$. Therefore, the particle number remains conserved for each momentum as expected for the Hamiltonian in Eq. (1) regardless of changes in chemical potential.

The result above reconciles two seemingly conflicting notions: (i) that chemical potential changes that are less than or of the order of the Mott gap are not expected to affect physical properties since the ground state is unchanged, and (ii) that only "occupied" singularities (zeros or poles) contribute to the total particle number. From our analysis above, we can conclude that indeed Green's function zeros contribute to the total particle number while also keeping it invariant to chemical potential changes smaller than $U$. The reconciliation between (i) and (ii) is made possible because properly accounting for zero contributions is necessary to obtain the correct invariant value, and any deviation of the topological quantity (here the Luttinger count $v_l$) from this value due to chemical potential changes is offset by an opposite variation of a nontopological one (here the backflow deviation $\delta v$) in Eq. (7). We will see below that a similar mechanism holds for the transverse Hall response function where the role of the Luttinger volume is played by the topological number $N_3$ [cf., Eqs. (35)–(37)].

## IV. HALL CONDUCTIVITY

In this section, we consider the electron transport properties in the presence of the Green's function zeros using the Kubo formula [52]. We reiterate that our analysis here of the

transverse Hall response is guided by the procedure we have used while considering the total charge in the previous section.

### A. Current operators

The (optical) conductivity can be evaluated by the correlation functions of current operators, which are derived from the continuity equations $\partial_t \rho + \nabla \cdot \boldsymbol{j} = \boldsymbol{0}$. Combining the Heisenberg equation of motion with the continuity equation, one is able to obtain the expression for the current operator as follows:

$$\boldsymbol{q} \cdot \boldsymbol{j}_{\boldsymbol{q}} = [H, \rho_{\boldsymbol{q}}], \tag{19}$$

in which the Fourier transformed density operator takes the following form:

$$\rho_{\boldsymbol{q}} = \frac{1}{\sqrt{N_L}} \sum_{\boldsymbol{k},\alpha\sigma} c^{\dagger}_{\boldsymbol{k}+\frac{\boldsymbol{q}}{2}\alpha\sigma} c_{\boldsymbol{k}-\frac{\boldsymbol{q}}{2}\alpha\sigma}. \tag{20}$$

Here $N_L$ stands for the size of the lattice. For a noninteracting Hamiltonian, the current operator is indeed the velocity operator of fermions:

$$\boldsymbol{J}_{\boldsymbol{q}} = \frac{1}{\sqrt{N_L}} \sum_{\boldsymbol{k},\alpha\sigma\beta\sigma'} \boldsymbol{v}_{\alpha\sigma,\beta\sigma'}(\boldsymbol{k}) c^{\dagger}_{\boldsymbol{k}+\frac{\boldsymbol{q}}{2}\alpha\sigma} c_{\boldsymbol{k}-\frac{\boldsymbol{q}}{2}\beta\sigma}, \tag{21}$$

in which $\boldsymbol{v}_{\alpha\sigma,\beta\sigma'}(\boldsymbol{k}) = \nabla_{\boldsymbol{k}} h_{\alpha\sigma,\beta\sigma'}(\boldsymbol{k})$ is the velocity matrix. However, when the interaction Hamiltonian contains terms that cannot be written as the products of local density operators (such as HK Hamiltonian), it will also contribute to the total current operator, which we will denote as $\boldsymbol{J}'_{\boldsymbol{q}}$:

$$\boldsymbol{q} \cdot \boldsymbol{J}'_{\boldsymbol{q}} = [H_I, \rho_{\boldsymbol{q}}], \tag{22}$$

and the total current is the summation of the two terms $\boldsymbol{j}_{\boldsymbol{q}} = \boldsymbol{J}_{\boldsymbol{q}} + \boldsymbol{J}'_{\boldsymbol{q}}$. Parameters in both the kinetic and interacting Hamiltonians will be affected by the external electromagnetic field $\boldsymbol{A}_{-\boldsymbol{q}}$ via Peierls substitution due to the gauge invariance, because the creation and annihilation operators in the interacting Hamiltonian are not always located on the same lattice sites in real space. As a consequence, the current operator $\boldsymbol{J}'_{\boldsymbol{q}}$ originating from the interacting Hamiltonian is also coupled to the gauge field. Similarly, the diamagnetic current can also originate from the interaction.

### B. Conductivity tensor

With all these factors considered, the optical conductivity with imaginary frequency can be written as a summation of the current-current susceptibility and the diamagnetic response from both $\boldsymbol{J}_{\boldsymbol{q}}$ and $\boldsymbol{J}'_{\boldsymbol{q}}$. More precisely, the conductivity tensor takes the following form:

$$\sigma_{ij}(\boldsymbol{q}, i\Omega) = \frac{1}{\Omega}(\mathcal{D}_{ij} + \chi_{ij}(\boldsymbol{q}, i\Omega) + \mathcal{D}'_{ij}(\boldsymbol{q}) + X_{ij}(\boldsymbol{q}, i\Omega)), \tag{23}$$

in which $\mathcal{D}_{ij}$ and $\mathcal{D}'_{ij}(\boldsymbol{q})$ are the diamagnetic response tensors obtained from expanding the kinetic Hamiltonian and interaction Hamiltonian to the second order of $\boldsymbol{A}_{\boldsymbol{q}}$, and the susceptibilities $\chi_{ij}$ and $X_{ij}$ are defined as follows:

$$\chi_{ij}(\boldsymbol{q}, i\Omega) = -\int d\tau\, e^{i\Omega\tau} \langle T_\tau j^i_{\boldsymbol{q}}(\tau) J^j_{-\boldsymbol{q}}(0) \rangle, \tag{24}$$

$$X_{ij}(\boldsymbol{q}, i\Omega) = -\int d\tau\, e^{i\Omega\tau} \langle T_\tau j^i_{\boldsymbol{q}}(\tau) J'^j_{-\boldsymbol{q}}(0) \rangle. \tag{25}$$

Since the interaction Hamiltonian usually contains four-fermion terms, the susceptibility $X_{ij}(\boldsymbol{q}, i\Omega)$ could contain correlation functions with more than six fermionic operators. Using the Ward-Takahashi identity [53,54], we are able to rewrite the susceptibility $\chi_{ij}$ together with the diamagnetic term $\mathcal{D}_{ij}$ as a charge-current susceptibility:

$$\mathcal{D}_{ij} + \lim_{\boldsymbol{q}\to 0} \chi_{ij}(\boldsymbol{q}, \Omega) = -i\Omega \lim_{\boldsymbol{q}\to 0} \frac{\partial}{\partial q_i} \chi_{0j}(\boldsymbol{q}, \Omega), \tag{26}$$

$$\chi_{0j}(\boldsymbol{q}, i\Omega) = -\int d\tau e^{i\Omega\tau} \langle T_\tau \rho_{\boldsymbol{q}}(\tau) J^j_{-\boldsymbol{q}}(0) \rangle. \tag{27}$$

The derivation of this relationship can be found in Appendix A. Thus, the conductivity tensor will contain the charge-current susceptibility as follows:

$$\sigma_{ij}(\boldsymbol{q} \to \boldsymbol{0}, i\Omega) = -i \lim_{\boldsymbol{q}\to 0} \frac{\partial}{\partial q_i} \chi_{0j}(\boldsymbol{q}, i\Omega) + \sigma'_{ij}(\boldsymbol{q}, i\Omega), \tag{28}$$

where $\sigma'_{ij}(\boldsymbol{q}, i\Omega)$ stands for the contributions from $\mathcal{D}'_{ij}(\boldsymbol{q})$ and $X_{ij}(\boldsymbol{q}, i\Omega)$, which contain correlation functions with six or more fermionic operators. To find the connection between the conductivity tensor and the Green's functions, it is better to write the charge-current susceptibility $\chi_{0j}$ as an integral of exact Green's functions $G(\boldsymbol{k}, i\omega)$ and the exact vertex function $\Lambda^0(\boldsymbol{q}, i\Omega; \boldsymbol{k}, i\omega)$ (the definition of which can be found in Appendix A):

$$\chi_{0j}(\boldsymbol{q}, i\Omega) = \frac{1}{\sqrt{N_L}} \sum_{\boldsymbol{k}} \int \frac{d\omega}{2\pi} \mathrm{Tr}\Big[ G\Big(\boldsymbol{k} + \frac{\boldsymbol{q}}{2}, i\omega\Big) \times \Lambda^0(\boldsymbol{k}, i\omega; \boldsymbol{q}, i\Omega) G\Big(\boldsymbol{k} - \frac{\boldsymbol{q}}{2}, i\omega + i\Omega\Big) v^j(\boldsymbol{k}) \Big]. \tag{29}$$

Taking the derivative of the susceptibility $\chi_{0j}$ with respect to the wave vector $\boldsymbol{q}$, we yield the following expression for the conductivity tensor:

$$\begin{aligned}
\sigma_{ij}(i\Omega) = &-i\frac{1}{\sqrt{N_L}} \sum_{\boldsymbol{k}} \int \frac{d\omega}{2\pi} \mathrm{Tr}\Big[ G(\boldsymbol{k}, i\omega) \frac{\partial \Lambda^0(\boldsymbol{k}, i\omega; \boldsymbol{q}, i\Omega)}{\partial q_i}\Big|_{\boldsymbol{q}\to 0} G(\boldsymbol{k}, i\omega + i\Omega) v^j(\boldsymbol{k}) \Big] \\
&- \frac{i}{2\sqrt{N_L}} \sum_{\boldsymbol{k}} \int \frac{d\omega}{2\pi} \mathrm{Tr}\Big[ \frac{\partial G(\boldsymbol{k}, i\omega)}{\partial k_i} \Lambda^0(\boldsymbol{k}, i\omega; \boldsymbol{q} \to \boldsymbol{0}, i\Omega) G(\boldsymbol{k}, i\omega + i\Omega) v^j(\boldsymbol{k}) \Big] \\
&+ \frac{i}{2\sqrt{N_L}} \sum_{\boldsymbol{k}} \int \frac{d\omega}{2\pi} \mathrm{Tr}\Big[ G(\boldsymbol{k}, i\omega) \Lambda^0(\boldsymbol{k}, i\omega; \boldsymbol{q} \to \boldsymbol{0}, i\Omega) \frac{\partial G(\boldsymbol{k}, i\omega + i\Omega)}{\partial k_i} v^j(\boldsymbol{k}) \Big] + \sigma'_{ij}(\boldsymbol{q}, i\Omega).
\end{aligned} \tag{30}$$

One can easily notice that the second and third terms only contain the vertex function $\Lambda^0$ at $\boldsymbol{q} \to \boldsymbol{0}$. Using the Ward-Takahashi identity for $\Lambda^\mu$, we are able to solve the vertex function $\Lambda^0(\boldsymbol{k}, i\omega; 0, i\Omega)$ as follows:

$$-i\Omega \cdot \Lambda^0(\boldsymbol{k}, i\omega; \boldsymbol{q} \to \boldsymbol{0}, i\Omega) = \frac{[G^{-1}(\boldsymbol{k}, i\omega) - G^{-1}(\boldsymbol{k}, i\omega + i\Omega)]}{\sqrt{N_L}} + \lim_{\boldsymbol{q}\to 0} \sum_i q_i \Lambda^i(\boldsymbol{q}, i\Omega; \boldsymbol{k}, i\omega)\,. \tag{31}$$

Here the second term will vanish if the vertex functions $\Lambda^i$ do not diverge at $\boldsymbol{q} = \boldsymbol{0}$. In normal condensed-matter systems with short-range interaction, this condition is usually satisfied. Because the HK model has a long-range interaction, we have, for generality, kept this term in the consideration. In the DC limit $i\Omega \to 0$, it can also be written as

$$\Lambda^0(\boldsymbol{k}, i\omega; \boldsymbol{q} \to \boldsymbol{0}, i\Omega \to 0) = -i\frac{1}{\sqrt{N_L}} \frac{\partial G^{-1}(\boldsymbol{k}, i\omega)}{\partial \omega} + \mathcal{F}(\boldsymbol{k}, i\omega), \tag{32}$$

$$\mathcal{F}(\boldsymbol{k}, i\omega) = \lim_{\Omega\to 0} \lim_{\boldsymbol{q}\to 0} \sum_i \frac{q_i}{-i\Omega} \Lambda^i(\boldsymbol{q}, i\Omega; \boldsymbol{k}, i\omega). \tag{33}$$

Using Eq. (32), the conductivity at the DC limit can be written as

$$\begin{aligned}
\sigma_{ij} = &-i\frac{1}{\sqrt{N_L}} \sum_{\boldsymbol{k}} \int \frac{d\omega}{2\pi} \mathrm{Tr}\left[ G(\boldsymbol{k}, i\omega) \frac{\partial \Lambda^0(\boldsymbol{k}, i\omega; \boldsymbol{q}, i\Omega \to 0)}{\partial q_i}\Big|_{q_i\to 0} G(\boldsymbol{k}, i\omega) v^j(\boldsymbol{k}) \right] \\
&- \frac{i}{2\sqrt{N_L}} \sum_{\boldsymbol{k}} \int \frac{d\omega}{2\pi} \mathrm{Tr}\left[ \frac{\partial G(\boldsymbol{k}, i\omega)}{\partial k_i} \mathcal{F}(\boldsymbol{k}, i\omega) G(\boldsymbol{k}, i\omega) v^j(\boldsymbol{k}) \right] \\
&+ \frac{i}{2\sqrt{N_L}} \sum_{\boldsymbol{k}} \int \frac{d\omega}{2\pi} \mathrm{Tr}\left[ \partial G(\boldsymbol{k}, i\omega) \mathcal{F}(\boldsymbol{k}, i\omega) \frac{\partial G(\boldsymbol{k}, i\omega)}{\partial k_i} v^j(\boldsymbol{k}) \right] \\
&- \frac{1}{2N_L} \sum_{\boldsymbol{k}} \int \frac{d\omega}{2\pi} \mathrm{Tr}\left[ \frac{\partial G(\boldsymbol{k}, i\omega)}{\partial k_i} \frac{\partial G^{-1}(\boldsymbol{k}, i\omega)}{\partial \omega} G(\boldsymbol{k}, i\omega) v^j(\boldsymbol{k}) \right] \\
&+ \frac{1}{2N_L} \sum_{\boldsymbol{k}} \int \frac{d\omega}{2\pi} \mathrm{Tr}\left[ G(\boldsymbol{k}, i\omega) \frac{\partial G^{-1}(\boldsymbol{k}, i\omega)}{\partial \omega} \frac{\partial G(\boldsymbol{k}, i\omega)}{\partial k_i} v^j(\boldsymbol{k}) \right] + \sigma'_{ij}(\boldsymbol{q}, i\Omega).
\end{aligned} \tag{34}$$

In addition to the $\sigma'_{ij}$ term from higher point correlation functions, Eq. (34) contains the information of the vertex functions $\Lambda^\mu$ at nonzero $\boldsymbol{q}$, which are inherently multipoint correlation functions and *cannot* be represented by Green's functions.

### C. $N_3$ and Hall conductivity

We focus on the Hall conductivity $\sigma_{xy}$ in this subsection. By using the identities $\partial G = -G\partial G^{-1} G$ and $v^j(\boldsymbol{k}) = -\partial_{k_j} G^{-1}(\boldsymbol{k}, i\omega) - \partial_{k_j} \Sigma(\boldsymbol{k}, i\omega)$, we are able to represent the velocity matrices and the derivatives of the Green function as the derivatives of Green's function inverse matrices. Thus, the expression of the Hall conductivity can be rewritten as [in analogy to Eq. (7) for the total particle number]

$$\sigma_{xy} = N_3 + \Delta N_3, \tag{35}$$

where the topological invariant

$$\begin{aligned}
N_3 = &\frac{1}{2N_L} \sum_{\boldsymbol{k}} \int \frac{d\omega}{2\pi} \mathrm{Tr}[G(\boldsymbol{k}, i\omega) \partial_\omega G^{-1}(\boldsymbol{k}, i\omega) G(\boldsymbol{k}, i\omega) \partial_{k_x} G^{-1}(\boldsymbol{k}, i\omega) G(\boldsymbol{k}, i\omega) \partial_{k_y} G^{-1}(\boldsymbol{k}, i\omega)] \\
&- \frac{1}{2N_L} \sum_{\boldsymbol{k}} \int \frac{d\omega}{2\pi} \mathrm{Tr}[G(\boldsymbol{k}, i\omega) \partial_{k_x} G^{-1}(\boldsymbol{k}, i\omega) G(\boldsymbol{k}, i\omega) \partial_\omega G^{-1}(\boldsymbol{k}, i\omega) G(\boldsymbol{k}, i\omega) \partial_{k_y} G^{-1}(\boldsymbol{k}, i\omega)]
\end{aligned} \tag{36}$$

gives the Hall conductivity in the noninteracting limit. The difference,

$$\begin{aligned}
\Delta N_3 = &-i\frac{1}{\sqrt{N_L}} \sum_{\boldsymbol{k}} \int \frac{d\omega}{2\pi} \mathrm{Tr}\left[ G(\boldsymbol{k}, i\omega) \frac{\partial \Lambda^0(\boldsymbol{k}, i\omega; \boldsymbol{q}, i\Omega \to 0)}{\partial q_x}\Big|_{q_x\to 0} G(\boldsymbol{k}, i\omega) v^y(\boldsymbol{k}) \right] \\
&- \frac{i}{2\sqrt{N_L}} \sum_{\boldsymbol{k}} \int \frac{d\omega}{2\pi} \mathrm{Tr}\left[ \frac{\partial G(\boldsymbol{k}, i\omega)}{\partial k_i} \mathcal{F}(\boldsymbol{k}, i\omega) G(\boldsymbol{k}, i\omega) v^j(\boldsymbol{k}) \right]
\end{aligned}$$

$$+\frac{i}{2\sqrt{N_L}}\sum_{\boldsymbol{k}}\int\frac{d\omega}{2\pi}\mathrm{Tr}\left[\partial G(\boldsymbol{k},i\omega)\mathcal{F}(\boldsymbol{k},i\omega)\frac{\partial G(\boldsymbol{k},i\omega)}{\partial k_i}v^j(\boldsymbol{k})\right]$$
$$+\frac{1}{2N_L}\sum_{\boldsymbol{k}}\int\frac{d\omega}{2\pi}\mathrm{Tr}[G(\boldsymbol{k},i\omega)\partial_\omega G^{-1}(\boldsymbol{k},i\omega)G(\boldsymbol{k},i\omega)\partial_{k_x}G^{-1}(\boldsymbol{k},i\omega)G(\boldsymbol{k},i\omega)\partial_{k_y}\Sigma(\boldsymbol{k},i\omega)]$$
$$-\frac{1}{2N_L}\sum_{\boldsymbol{k}}\int\frac{d\omega}{2\pi}\mathrm{Tr}[G(\boldsymbol{k},i\omega)\partial_{k_x}G^{-1}(\boldsymbol{k},i\omega)G(\boldsymbol{k},i\omega)\partial_\omega G^{-1}(\boldsymbol{k},i\omega)G(\boldsymbol{k},i\omega)\partial_{k_y}\Sigma(\boldsymbol{k},i\omega)]+\sigma'_{ij}(\boldsymbol{q},i\Omega), \tag{37}$$

is an analog to $\delta v$ in the generalized Luttinger's theorem, and it vanishes in the absence of interactions. Specifically, in the noninteracting limit, the self-energy $\Sigma(\boldsymbol{k},i\omega)$ is zero, and the vertex function is a constant matrix $\Lambda^0(\boldsymbol{k},i\omega;\boldsymbol{q},i\Omega)=\mathbb{1}/\sqrt{N_L}$ because of *Wick's theorem* (instead of a consequence of the Ward-Takahashi identity). The contribution from six- or-more-point correlation functions $\sigma'_{ij}(\boldsymbol{q},i\Omega)$ also vanishes since $\boldsymbol{J}'_{\boldsymbol{q}}=\boldsymbol{0}$. Thus, all the terms in the expression of $\Delta N_3$ are zero, which indicates $\sigma_{xy}=N_3$. However, in the presence of interactions, the vertex $\Lambda^0$ is no longer a constant function of $\boldsymbol{q}$, and the self-energy $\Sigma(\boldsymbol{k},i\omega)\neq 0$, and in general we cannot identify the topological index $N_3$ as the Hall conductivity. The vertex functions $\Lambda^0$ inherently encode a four-point function, and the Ward-Takahashi identity is only able to relate it to *both* the Green's functions and other vertex functions together, rather than representing everything solely through the Green's function.

Nevertheless, both values of $N_3$ in $\Delta N_3$ receive contributions from the zeros of the Green's function, provided that interactions are properly accounted for. As exemplified by the Hatsugai-Kohmoto model, to be discussed below in Sec. IV D (see Fig. 4 and the associated text), $N_3$ contains terms that are affected by the number of zeros below the chemical potential. Thus the choice of chemical potential even within an insulating gap can modify $N_3$ in close analogy to the Luttinger volume $v_l$ in Eq. (7). While the Green's function zeros' contributions to $N_3$ have been highlighted in Refs. [30,39,40], we establish here such contributions in a consistent, gauge-invariant way. Therefore, caution must be exercised when considering Green's function zeros, particularly when computing observable quantities like $\sigma_{xy}$ using Green's functions and other correlation functions. Despite this, later in the next section, we will show how the zero-temperature conductivity remains unchanged under variations of the chemical potential within the Mott gap in the spirit of our previous discussion on the total charge.

A natural question regarding the Hall conductivity is whether $\sigma_{xy}$ will be equal to $N_3$ when $\Sigma(\boldsymbol{k},i\omega)=\Sigma(i\omega)$ is $\boldsymbol{k}$-independent. Indeed, such self-energy could eliminate the two terms in the fourth and fifth lines of Eq. (37), indicating that $\sigma_{xy}$ is different from $N_3$ by only a term containing $\Lambda^0$ and $\sigma'_{ij}(\boldsymbol{q},i\Omega)$, which contains six- or eight-point correlation functions [when the vector vertex functions are well-behaved in the long-wavelength limit, such that $\mathcal{F}(\boldsymbol{k},i\omega)=0$]. One may wonder if the derivative of the vertex function $\Lambda^0$ can be represented by Green's functions via the Ward-Takahashi identity. Since this remaining term contains the derivative of $\Lambda^0$ with respect to $\boldsymbol{q}$, we are not able to use Eq. (32) directly. In fact, one could check that the following ansatz vertex functions $\Lambda^\mu$ all satisfy the Ward-Takahashi identity:

$$\Lambda^0(\boldsymbol{k},i\omega;\boldsymbol{q},i\Omega\to 0)=\frac{1}{\sqrt{N_L}}\left(\mathbb{1}+i\frac{\Sigma(i\omega+i\Omega)-\Sigma(i\omega)}{\Omega}-\boldsymbol{q}\cdot\boldsymbol{\ell}\right), \tag{38}$$
$$\Lambda^i(\boldsymbol{k},i\omega,\boldsymbol{q},i\Omega\to 0)=\frac{1}{\sqrt{N_L}}(v^i(\boldsymbol{k})+i\Omega\cdot\ell_i). \tag{39}$$

Here $\boldsymbol{\ell}$ is a constant vector with the same dimension as length. The Ward-Takahashi identity is satisfied regardless of the choice of $\boldsymbol{\ell}$. Therefore, the derivative of the vertex function $\Lambda^0$ in the $\boldsymbol{q}\to\boldsymbol{0}$, $\Omega\to 0$ limit will be

$$\left.\frac{\partial\Lambda^0(\boldsymbol{k},i\omega;\boldsymbol{q},i\Omega\to 0)}{\partial q_x}\right|_{q_x\to 0}=-\frac{\ell_x}{\sqrt{N_L}}. \tag{40}$$

The value of $\ell_x$ is not able to be solely solved from the Ward-Takahashi identity. Thus, we cannot further reduce Eq. (37) into an expression that only contains full Green's functions, even if the self-energy $\Sigma$ is momentum $\boldsymbol{k}$-independent.

### D. HK model with Chern bands

HK models are easily solvable using numerically exact diagonalization even if the kinetic energy $h_{\alpha\sigma,\beta\sigma'}(\boldsymbol{k})$ is not diagonal, due to the presence of a huge amount of good quantum numbers $N_{\boldsymbol{k}}=\sum_{\alpha\sigma}c^\dagger_{\boldsymbol{k}\alpha\sigma}c_{\boldsymbol{k}\alpha\sigma}$. We choose a tight-binding lattice model that carries a nonzero Chern number. The corresponding Hamiltonian is given by

$$H_0=\sum_{\boldsymbol{k},\alpha\sigma,\beta\sigma'}h_{\alpha\sigma,\beta\sigma'}(\boldsymbol{k})c^\dagger_{\boldsymbol{k}\alpha\sigma}c_{\boldsymbol{k}\beta\sigma'}, \tag{41}$$
$$h(\boldsymbol{k})=[t_{12}(\tau_1\sin k_x+\tau_2\sin k_y)+\tau_3(M-t\cos k_x-t\cos k_y)]\otimes s_0, \tag{42}$$
$$H_I=\frac{U}{2}\sum_{\boldsymbol{k}}\sum_{\alpha=1}^{2}(n_{\boldsymbol{k}\alpha\uparrow}+n_{\boldsymbol{k}\alpha\downarrow}-1)^2. \tag{43}$$

Here we use $\tau_{0,1,2,3}$ to represent the identity and Pauli matrices with sublattice indices ($\alpha=1,2$), and we use $s_{0,1,2,3}$ to represent the identity and Pauli matrices with spin indices ($\sigma=\uparrow,\downarrow$). Since the kinetic Hamiltonian $h(\boldsymbol{k})$ is proportional to $s_0$, it has a spin SU(2) symmetry. When the parameters are chosen to be $t_{12}=t=1$ and $|M|<2$, the two energy bands of each spin will carry Chern numbers $\nu_C=\pm 1$, and due to the spin SU(2) symmetry of the whole kinetic Hamiltonian, the two lower energy bands have the same Chern number. In the numerical calculation, we will choose $M=1$. The Hamiltonians for every momentum value $H_{\boldsymbol{k}}$ are completely decoupled from each other. Hence, the spectra and the wave functions for

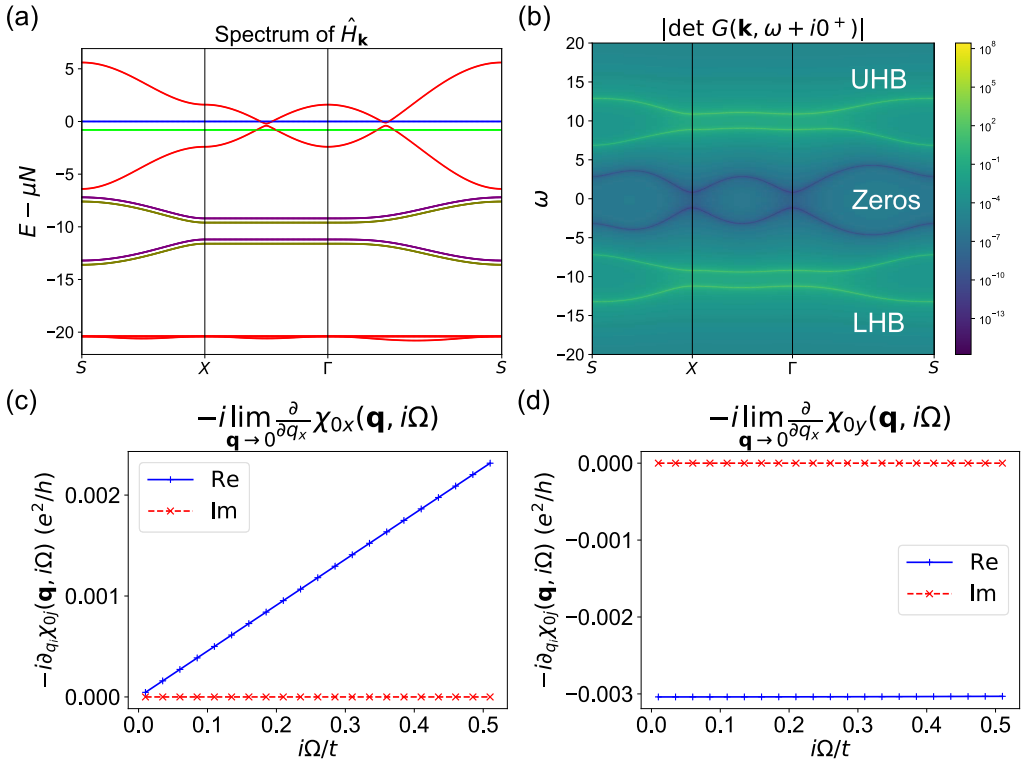


FIG. 3. (a) The many-body energy spectrum of $H_k - \mu N_k$ along the high-symmetry lines. Here we choose $t_{12} = t = 1$, $M = 1$, and $U = 20$. States with electron numbers $N_k = 0, 1, 2, 3, 4$ are labeled by blue, purple, red, brown, and green, respectively. In this figure we also added a chemical potential $\mu = 0.2$ to separate the $N_k = 1$ and 3 states. (b) The Green's function determinant $|\det G(\boldsymbol{k}, \omega + i0^+)|$ along the high-symmetry lines. The corresponding value of $N_3$ computed from this Green's function is $N_3 = -2$. (c),(d) Longitudinal and transverse components of the tensor $-i\lim_{\boldsymbol{q}\to 0}\partial_{q_i}\chi_{0j}(\boldsymbol{q}, i\Omega)$ as functions of imaginary frequency. The conductivity tensor $\sigma_{ij}$ is different from this quantity by $\sigma'_{ij}(\boldsymbol{q}, i\Omega)$ as shown in Eq. (28). The real part value of $-i\lim_{\boldsymbol{q}\to 0}\partial_{q_x}\chi_{0y}(\boldsymbol{q}, i\Omega)$ at zero frequency is clearly different from the value of $N_3$, indicating that the backflow term $\Delta N_3$ is nonzero.

each $H_k$ can be numerically solved easily, since it is a $16 \times 16$ matrix. In Fig. 3(a), we provide the energy spectra of $H_k - \mu N_k$ when the chemical potential is tuned such that the ground state is at half-filling. We also note that the ground state for each $\boldsymbol{k}$ will not change if the chemical potential is changed by a value $|\Delta\mu| \ll U/2$, due to the gap between the ground states ($N_k = 2$) and the charge $\pm 1$ ($N_k = 1, 3$) excitations.

The many-body wave functions of the whole system are simply the tensor products of the wave functions for each $\boldsymbol{k}$. With these exact wave functions in hand, we are able to compute quantities, such as Green's functions and susceptibilities via spectral decomposition. The determinant of the Green's function along high-symmetry lines can be found in Fig. 3(b). Dispersive poles and zeros with different dispersion relationships are clearly visible. We also find numerically the topological index $N_3 = -2$ for this Green's function.

The derivative of the charge-current susceptibility $\chi_{0j}(\boldsymbol{q}, i\Omega)$, which has been shown to be an important part of the conductivity tensor $\sigma_{ij}$, can also be evaluated numerically using spectral decomposition, as we discuss in Appendix B. Figures 3(c) and 3(d) provide the values of the $xx$ and $xy$ components of $-i\lim_{\boldsymbol{q}\to 0}\partial_{q_i}\chi_{0j}(\boldsymbol{q}, i\Omega)$ with imaginary frequencies. Clearly, the transverse component of this quantity is a nonzero small value. However, it is far from the value of $N_3$, a plot of which appears in Fig. 4 for the HK model. Thus, we can conclude that the backflow terms $\Delta N_3$ in Eq. (37) are not negligible even if $\sigma'_{xy}$ does not contribute.

We now comment on the extra term $\sigma'_{ij}(\boldsymbol{q}, i\Omega)$ in the expression of the total conductivity tensor, which describes the current $\boldsymbol{j_q}$ response from the coupling term between the ex-

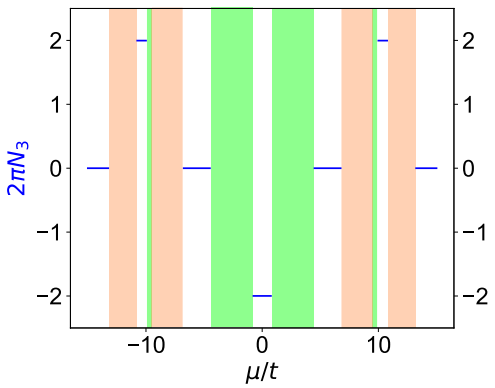


FIG. 4. Variation of the topological winding number $N_3$ as a function of the chemical potential normalized by the hopping $t$. The zero (pole) bands are shown in green (orange) while the horizontal blue lines denote the values of $N_3$. $N_3$ is ill-defined in the energy windows where the zero and pole bands occur. The Mott gap is set to $20t$.

ternal gauge field and the interaction current operator $\boldsymbol{J}'_{-\boldsymbol{q}}$. As we have already mentioned, this term is inherently a six-and-more-point correlation function, and it cannot be represented by the exact Green's function. It amounts to an extra contribution to the backflow term $\Delta N_3$.

Finally, we now show why the conductivity at zero temperature remains unchanged under variations in the chemical potential, provided that such changes do not alter the ground state. For the HK Hamiltonian at half-filling, the ground state for each $\boldsymbol{k}$ has a large gap $\sim U/2$ from any charge excitations, and as a consequence, the many-body ground states will remain in the half-filling sector in a range of chemical potential. As we specified in Eq. (23), the conductivity tensor contains the current-current susceptibility, which can be expressed in terms of a spectral decomposition:

$$\begin{aligned}&\chi_{ij}(\boldsymbol{q}, i\Omega) + X_{ij}(\boldsymbol{q}, i\Omega)\\ &= \frac{1}{|\mathcal{G}|}\sum_{g\in\mathcal{G},m}\left[\frac{\langle g|j^i_{\boldsymbol{q}}|m\rangle\langle m|j^j_{-\boldsymbol{q}}|g\rangle}{i\Omega + (E_g - \mu N_g) - (E_m - \mu N_m)}\right.\\ &\quad\left. - \frac{\langle g|j^j_{-\boldsymbol{q}}|m\rangle\langle m|j^i_{\boldsymbol{q}}|g\rangle}{i\Omega - (E_g - \mu N_g) + (E_m - \mu N_m)}\right].\end{aligned} \tag{44}$$

Here, $\mathcal{G}$ denotes the set of degenerate ground states, and $|\mathcal{G}|$ stands for the ground state degeneracy. In addition, $E_g, E_m$ and $N_g, N_m$ stand for the eigenvalues of the many-body Hamiltonian and the fermion number operator of many-body eigenstates $|g\rangle$ and $|m\rangle$, respectively. The current operators $\boldsymbol{j}_{\boldsymbol{q}}$ always contain the same amount of fermion creation and annihilation operators. As a consequence, any excited state $|m\rangle$ that satisfies $\langle g|j^i_{\boldsymbol{q}}|m\rangle \neq 0$ must have the same fermion number eigenvalue ($N_g = N_m$). Hence, the chemical potential $\mu$ does not show up in the denominator. If the ground states $|g\rangle$ remain unchanged when varying $\mu$ (which is true for a charge gapped system), Eq. (44) will also remain unchanged, regardless of whether the Green's function zeros are at the Fermi level or not. Meanwhile, the diamagnetic response tensors $\mathcal{D}_{ij}$ and $\mathcal{D}'_{ij}(\boldsymbol{q})$ are directly determined by the ground-state expectation values of fermionic operator products, which are unchanged if the ground state remains the same while changing $\mu$ even if it passes through zeros. As a consequence, the conductivity tensor will not be changed as well. This is despite the following: (i) The value of $N_3$ can be changed by varying the chemical potential across zero bands. The variation of $N_3$ for the Hatsugai-Kohmoto model is shown numerically in Fig. 4, and it occurs even if the ground state is unaffected. (ii) $\sigma_{xy}$ must receive contributing terms from zeros that must be properly accounted for. We infer this from our numerical evaluation of $N_3$ for the HK model in Fig. 4 as well as Eqs. (35)–(37) in analogy to the total charge in Eq. (7). With these fully gauge-invariant calculations, we have thus demonstrated how zero contributions to both the total charge and Hall conductivity can be properly accounted for, while at the same time the physical observable itself remains invariant under chemical potential variations within the Mott gap. We stress that our emphasis here is not on the distinctness between the Hall conductivity and $N_3$ *per se* [40] but on the behavior of the Hall conductivity itself.

## V. DISCUSSION AND SUMMARY

Several remarks are in order. First, as stated in the Introduction, probing Green's function zeros experimentally is not a straightforward task. Our objective in this paper is to study how zeros *contribute* to certain observables in a consistent, gauge-invariant manner. Extracting this contribution unambiguously is a challenge and a subject of ongoing debate, which we postpone for a future investigation. A naive application of ordinary spectroscopic tools such as photoemission, tunneling, or x-ray/neutron scattering does not automatically reveal their existence, and a more nuanced approach is necessary. Instead, one might rely on specific probes that could extract this information more indirectly. For example, a key mechanism for the occurrence of zeros is through ground-state degeneracies, where we expect the zeros to come from a resonance scattering of electrons from singular collective spin excitations. In this regard, a Curie-like behavior of the static, long-wavelength magnetic susceptibility in the zero-field limit with a Mott gap is a strong indicator of Green's function zeros. In principle, processes connecting nondegenerate but mixed ground states to excited states can also yield zeros at zero temperature. Such scenarios must be treated on a case-by-case basis. Second, in the current paper we have not derived explicit forms of the six-and-more-point correlation functions dictated by gauge invariance and alluded to in Eq. (30). These terms contribute to the deviation of $\sigma_{xy}$ from its topological invariant $N_3$ as its particle number counterpart in Eq. (7). Nonetheless, we are able to reach the key conclusion that measurable properties are contributed to by Green's function zeros while remaining unchanged with chemical potential up to the Mott scale.

In summary, in this work we have examined the role of quasiparticle loss on physical properties by studying an exactly solvable model of a Mott insulator. The model contains contours in momentum-frequency space where the Green's function vanishes to yield zeros within the Mott gap. We demonstrate that these zeros contribute to physical properties, such as the total particle number and conductivity tensor, in a way that is consistent with the expectations from general physical grounds. As an example of the latter, the observables are shown to be insensitive to changes in chemical potential within the Mott gap. Our results offer a conceptual framework for further analysis of topological response functions in strongly correlated systems and quantum materials where a well-defined quasiparticle picture is absent. As such, we expect our work to help further advance the understanding of the rich interplay among topology, symmetry, and strong correlations.

*Note added:* After completing this manuscript, we became aware of unpublished work in which the many-body effects of Hall conductivity are also addressed [39,55].

## ACKNOWLEDGMENTS

We thank Jennifer Cano, Elio König, Diana-Gabriela Oprea, Silke Paschen, and Roser Valenti for useful discussions. Work at Rice has primarily been supported by the Air Force Office of Scientific Research under Grant No. FA9550-21-1-0356 (C.S. and S.S.), by the National Science Foundation under Grant No. DMR-2220603

(F.X. and L.C.), and by the Robert A. Welch Foundation Grant No. C-1411 and the Vannevar Bush Faculty Fellowship ONR-VB N00014-23-1-2870 (Q.S.). The majority of the computational calculations have been performed on the Shared University Grid at Rice funded by NSF under Grant EIA-0216467, a partnership between Rice University, Sun Microsystems, and Sigma Solutions, Inc., the Big-Data Private-Cloud Research Cyberinfrastructure MRI-award funded by NSF under Grant No. CNS-1338099, and the Extreme Science and Engineering Discovery Environment (XSEDE) by NSF under Grant No. DMR170109. M.G.V. acknowledges support of the Deutsche Forschungsgemeinschaft (DFG, German Research Foundation) GA 3314/1-1 - FOR 5249 (QUAST) and partial support from European Research Council (ERC) Grant Agreement No. 101020833. This work has also been funded by the European Union NextGenerationEU/PRTR-C17.I1, as well as by the IKUR Strategy under the collaboration agreement between Ikerbasque Foundation and DIPC on behalf of the Department of Education of the Basque Government. All authors acknowledge the hospitality of the Kavli Institute for Theoretical Physics, UCSB, supported in part by the National Science Foundation under Grant No. NSF PHY-1748958, during the program "A Quantum Universe in a Crystal: Symmetry and Topology across the Correlation Spectrum." Q.S. and S.S. also acknowledge the hospitality of the Aspen Center for Physics, which is supported by the National Science Foundation under Grant No. PHY-2210452, during the workshop "New Directions on Strange Metals in Correlated Systems." C.S. acknowledges partial support from Iowa State University startup funds.

C.S. and F.X. contributed equally to this work.

## APPENDIX A: WARD-TAKAHASHI IDENTITY AND SUSCEPTIBILITIES

In this Appendix, we provide a detailed discussion regarding the susceptibilities $\chi_{ij}$, $\chi_{0j}$ and the relationship between these susceptibilities and the Ward identity [53,54].

The Ward-Takahashi identity can be formulated into the following form using imaginary-time representation:

$$\begin{aligned}&\partial_\tau\left\langle T_\tau \rho_{\boldsymbol{q}}(\tau) c^\dagger_{\boldsymbol{k}-\frac{\boldsymbol{q}}{2}\alpha\sigma}(\tau') c_{\boldsymbol{k}+\frac{\boldsymbol{q}}{2}\beta\sigma'}(\tau'')\right\rangle \\ &\quad = \boldsymbol{q}\cdot\left\langle T_\tau \boldsymbol{j}_{\boldsymbol{q}}(\tau) c^\dagger_{\boldsymbol{k}-\frac{\boldsymbol{q}}{2}\alpha\sigma}(\tau') c_{\boldsymbol{k}+\frac{\boldsymbol{q}}{2}\beta\sigma'}(\tau'')\right\rangle + \frac{\delta(\tau'-\tau)}{\sqrt{N_L}} G_{\beta\sigma',\alpha\sigma}\left(\boldsymbol{k}+\frac{\boldsymbol{q}}{2}, \tau''-\tau\right) - \frac{\delta(\tau''-\tau)}{\sqrt{N_L}} G_{\beta\sigma',\alpha\sigma}\left(\boldsymbol{k}-\frac{\boldsymbol{q}}{2}, \tau-\tau'\right),\end{aligned} \tag{A1}$$

in which $G_{\beta\sigma',\alpha\sigma}(\boldsymbol{k},\tau) = -\langle T_\tau c_{\boldsymbol{k},\beta\sigma'}(\tau) c^\dagger_{\boldsymbol{k},\alpha\sigma}(0)\rangle$ represents the imaginary-time Green's function. This identity can also be written in the frequency domain by performing the Fourier transformation on both sides. A compact way to rewrite the frequency-domain Ward-Takahashi identity is

$$-i\Omega\cdot Q^0_{\alpha\sigma,\beta\sigma'}(\boldsymbol{k}, i\omega; \boldsymbol{q}, i\Omega) = \boldsymbol{q}\cdot\boldsymbol{Q}_{\alpha\sigma,\beta\sigma'}(\boldsymbol{k}, i\omega; \boldsymbol{q}, i\Omega) + \frac{1}{\sqrt{N_L}} G_{\beta\sigma',\alpha\sigma}\left(\boldsymbol{k}+\frac{\boldsymbol{q}}{2}, i\omega\right) - \frac{1}{\sqrt{N_L}} G_{\beta\sigma',\alpha\sigma}\left(\boldsymbol{k}-\frac{\boldsymbol{q}}{2}, i\omega+i\Omega\right), \tag{A2}$$

in which the correlation functions $Q^\mu_{\alpha\sigma,\beta\sigma'}(\boldsymbol{k}, i\omega; \boldsymbol{q}, i\Omega)$ are defined as

$$Q^0_{\alpha\sigma,\beta\sigma'}(\boldsymbol{k}, i\omega; \boldsymbol{q}, i\Omega) = \int d\tau \int d\tau'' e^{i(\Omega\tau+\omega\tau'')}\left\langle T_\tau \rho_{\boldsymbol{q}}(\tau) c^\dagger_{\boldsymbol{k}-\frac{\boldsymbol{q}}{2}\alpha\sigma}(0) c_{\boldsymbol{k}+\frac{\boldsymbol{q}}{2}\beta\sigma'}(\tau'')\right\rangle, \tag{A3}$$

$$Q^i_{\alpha\sigma,\beta\sigma'}(\boldsymbol{k}, i\omega; \boldsymbol{q}, i\Omega) = \int d\tau \int d\tau'' e^{i(\Omega\tau+\omega\tau'')}\left\langle T_\tau j^i_{\boldsymbol{q}}(\tau) c^\dagger_{\boldsymbol{k}-\frac{\boldsymbol{q}}{2}\alpha\sigma}(0) c_{\boldsymbol{k}+\frac{\boldsymbol{q}}{2}\beta\sigma'}(\tau'')\right\rangle. \tag{A4}$$

Another useful form of the Ward-Takahashi identity connects the Green's functions and vertex functions $\Lambda^\mu(\boldsymbol{q}, i\Omega; \boldsymbol{k}, i\omega)$, which are defined as

$$\Lambda^\mu(\boldsymbol{k}, i\omega; \boldsymbol{q}, i\Omega) = -G^{-1}\left(\boldsymbol{k}+\frac{\boldsymbol{q}}{2}, i\omega\right)[Q^\mu(\boldsymbol{k}, i\omega; \boldsymbol{q}, i\Omega)]^{\mathrm{T}} G^{-1}\left(\boldsymbol{k}-\frac{\boldsymbol{q}}{2}, i\omega+i\Omega\right). \tag{A5}$$

Thus, we can obtain the Ward-Takahashi identity using the vertex functions by rewriting Eq. (A2),

$$-i\Omega\cdot\Lambda^0(\boldsymbol{k}, i\omega; \boldsymbol{q}, i\Omega) = \sum_i q_i\cdot\Lambda^i(\boldsymbol{k}, i\omega; \boldsymbol{q}, i\Omega) - \frac{1}{\sqrt{N_L}}\left[G^{-1}\left(\boldsymbol{k}-\frac{\boldsymbol{q}}{2}, i\omega+i\Omega\right) - G^{-1}\left(\boldsymbol{k}+\frac{\boldsymbol{q}}{2}, i\omega\right)\right]. \tag{A6}$$

It is obvious that the susceptibilities $\chi_{ij}(\boldsymbol{q}, i\Omega)$ and $\chi_{0j}(\boldsymbol{q}, i\Omega)$, which are defined in Eqs. (24) and (27), can be represented by the correlation functions $Q^\mu(\boldsymbol{q}, i\Omega; \boldsymbol{k}, i\omega)$ in the following form:

$$\chi_{0j}(\boldsymbol{q}, i\Omega) = -\int d\tau e^{i\Omega\tau}\left\langle T_\tau \rho_{\boldsymbol{q}}(\tau) J^j_{-\boldsymbol{q}}(0)\right\rangle = -\frac{1}{\sqrt{N_L}}\sum_{\boldsymbol{k}}\int\frac{d\omega}{2\pi}\mathrm{Tr}[(Q^0(\boldsymbol{k}, i\omega; \boldsymbol{q}, i\Omega))^{\mathrm{T}} v^j(\boldsymbol{k})], \tag{A7}$$

$$\chi_{ij}(\boldsymbol{q}, i\Omega) = -\int d\tau e^{i\Omega\tau}\left\langle T_\tau j^i_{\boldsymbol{q}}(\tau) J^j_{-\boldsymbol{q}}(0)\right\rangle = -\frac{1}{\sqrt{N_L}}\sum_{\boldsymbol{k}}\int\frac{d\omega}{2\pi}\mathrm{Tr}[(Q^i(\boldsymbol{k}, i\omega; \boldsymbol{q}, i\Omega))^{\mathrm{T}} v^j(\boldsymbol{k})]. \tag{A8}$$

Combining this with the Ward-Takahashi identity shown in Eq. (A2), we can find how these two susceptibilities are related to the Green's functions:

$$-i\Omega\cdot\chi_{0j}(\boldsymbol{q},i\Omega)=\sum_i q_i\chi_{ij}(\boldsymbol{q},i\Omega)-\int_{\mathrm{BZ}}\frac{d^dk}{(2\pi)^d}\int\frac{d\omega}{2\pi}\mathrm{Tr}\left[\frac{\partial h(\boldsymbol{k})}{\partial k_j}\left[G\left(\boldsymbol{k}+\frac{\boldsymbol{q}}{2},i\omega\right)-G\left(\boldsymbol{k}-\frac{\boldsymbol{q}}{2},i\omega+i\Omega\right)\right]\right]. \tag{A9}$$

By taking the derivative with respect to $q_i$ and then taking the $\boldsymbol{q}\to\boldsymbol{0}$ limit, we are able to obtain the expression for the $\chi_{ij}(\boldsymbol{q},i\Omega)$ as shown:

$$\chi_{ij}(\boldsymbol{q}\to\boldsymbol{0},i\Omega)=-i\Omega\lim_{\boldsymbol{q}\to0}\frac{\partial}{\partial q_i}\chi_{0j}(\boldsymbol{q},i\Omega)+\int_{\mathrm{BZ}}\frac{d^dk}{(2\pi)^d}\int\frac{d\omega}{2\pi}\mathrm{Tr}\left[\frac{1}{2}\frac{\partial h(\boldsymbol{k})}{\partial k_j}\frac{\partial}{\partial k_i}(G(\boldsymbol{k},i\omega)+G(\boldsymbol{k},i\omega+i\Omega))\right]. \tag{A10}$$

If the integral over $\omega$ in the second term is *absolute convergent*, it will not depend on the value of $\Omega$, since it is equivalent to a shift of the variable of integration $\omega\to\omega+\Omega$. Hence, Eq. (A10) can be further simplified into

$$\chi_{ij}(\boldsymbol{q}\to\boldsymbol{0},i\Omega)=-i\Omega\lim_{\boldsymbol{q}\to0}\frac{\partial}{\partial q_i}\chi_{0j}(\boldsymbol{q},i\Omega)+\int_{\mathrm{BZ}}\frac{d^dk}{(2\pi)^d}\int\frac{d\omega}{2\pi}\mathrm{Tr}\left[\frac{\partial h(\boldsymbol{k})}{\partial k_j}\frac{\partial G(\boldsymbol{k},i\omega)}{\partial k_i}\right]. \tag{A11}$$

Using this equation, we are able to show that Eq. (26) in the main text will hold if the Ward-Takahashi identity is satisfied. The diamagnetic response tensor from the kinetic Hamiltonian $\mathcal{D}_{ij}$ has the following form:

$$\mathcal{D}_{ij}=\int_{\mathrm{BZ}}\frac{d^dk}{(2\pi)^d}\sum_{\alpha\sigma\beta\sigma'}\frac{\partial^2h_{\alpha\sigma,\beta\sigma'}(\boldsymbol{k})}{\partial k_i\partial k_j}\langle g|c^\dagger_{\boldsymbol{k}\alpha\sigma}c_{\boldsymbol{k}\beta\sigma'}|g\rangle. \tag{A12}$$

We can use the Green's functions to represent the fermion operator bilinear expectation values, which have been used in the proof of Luttinger theorem [33]:

$$\langle g|c^\dagger_{\boldsymbol{k}\alpha\sigma}c_{\boldsymbol{k}\beta\sigma'}|g\rangle=G_{\beta\sigma',\alpha\sigma}(\boldsymbol{k},\tau=0^-)=\int\frac{d\omega}{2\pi}G_{\beta\sigma',\alpha\sigma}(\boldsymbol{k},i\omega)e^{i\omega0^+}, \tag{A13}$$

in which the factor $e^{i\omega0^+}$ ensures that the integrals for the diagonal elements ($\alpha\sigma=\beta\sigma'$) converge. By doing so, the diamagnetic response tensor becomes

$$\mathcal{D}_{ij}=\int_{\mathrm{BZ}}\frac{d^dk}{(2\pi)^d}\int\frac{d\omega}{2\pi}\mathrm{Tr}\left[\frac{\partial^2h(\boldsymbol{k})}{\partial k_i\partial k_j}G(\boldsymbol{k},i\omega)\right]e^{i\omega0^+}. \tag{A14}$$

By performing the integration by parts with respect to $k_i$, this expression can further be transformed into

$$\mathcal{D}_{ij}=\int_{\mathrm{BZ}}\frac{d^dk}{(2\pi)^d}\int\frac{d\omega}{2\pi}\mathrm{Tr}\left[\frac{\partial}{\partial k_i}\left(\frac{\partial h(\boldsymbol{k})}{\partial k_j}G(\boldsymbol{k},i\omega)\right)-\frac{\partial h(\boldsymbol{k})}{\partial k_j}\frac{\partial G(\boldsymbol{k},i\omega)}{\partial k_i}\right]e^{i\omega0^+}. \tag{A15}$$

The first term, being a derivative of $k_i$, will vanish, since the kinetic Hamiltonian $h(\boldsymbol{k})$ and the interacting Green's function $G(\boldsymbol{k},i\omega)$ are periodic functions in the whole Brillouin zone. Therefore, only the second term remains. Because we have assumed that the integral over $\omega$ of $\partial_{k_i}G(\boldsymbol{k},i\omega)$ is absolutely convergent, the infinitesimal exponential factor $e^{i\omega0^+}$ could be dropped. Thus, the diamagnetic response tensor exactly cancels the Green's function part in Eq. (A11). We conclude that the summation of the diamagnetic response $\mathcal{D}_{ij}$ and the susceptibility $\chi_{ij}(\boldsymbol{q}\to\boldsymbol{0},i\Omega)$ can be written as

$$\mathcal{D}_{ij}+\chi_{ij}(\boldsymbol{q}\to\boldsymbol{0},i\Omega)=-i\Omega\lim_{\boldsymbol{q}\to0}\frac{\partial}{\partial q_i}\chi_{0j}(\boldsymbol{q},i\Omega), \tag{A16}$$

which is indeed the form of Eq. (26) in the main text.

The above discussion is based on the assumption that the integral $\int d\omega\partial_{k_i}G(\boldsymbol{k},i\omega)$ is absolutely convergent. Here we argue that this is indeed true using the analytic properties of Green's functions. The derivative of the Green's function with respect to momentum $k_i$ can be reexpressed as

$$\frac{\partial G(\boldsymbol{k},z)}{\partial k_i}=-G(\boldsymbol{k},z)\frac{\partial G^{-1}(\boldsymbol{k},z)}{\partial k_i}G(\boldsymbol{k},i\omega)=G(\boldsymbol{k},z)\left[v(\boldsymbol{k})+\frac{\partial\Sigma(\boldsymbol{k},z)}{\partial k_i}\right]G(\boldsymbol{k},z), \tag{A17}$$

where $\Sigma(\boldsymbol{k},z)=z-h(\boldsymbol{k})-G^{-1}(\boldsymbol{k},z)$ is the self-energy. In general, an element of the Green's function at large frequency decays as or faster than $\frac{1}{z}$, or more precisely, $\lim_{z\to\infty}|z\cdot G_{\alpha\sigma,\beta\sigma'}(\boldsymbol{k},z)|\leqslant1$. At high frequency, self-energy becomes finite and frequency-independent [56], as does its derivative $\lim_{z\to\infty}|\partial_{k_i}\Sigma(\boldsymbol{k},z)|<\infty$. Therefore, each element of the derivative of the Green's function will satisfy the inequality

$$\lim_{z\to\infty}\left|z^2\frac{\partial G_{\alpha\sigma,\beta\sigma'}(\boldsymbol{k},z)}{\partial k_i}\right|<\infty. \tag{A18}$$

Since the absolute value of the integrand decays as or even faster than $\frac{1}{\omega^2}$, the integral over $\omega$ in Eq. (A10) is absolutely convergent.

## APPENDIX B: SPECTRAL DECOMPOSITION OF GREEN'S FUNCTION AND SUSCEPTIBILITIES IN HK MODELS

Since the electron numbers at each momentum point $\boldsymbol{k}$ are all conserved quantities, the many-body eigenstate wave functions can be built by the tensor products of eigenstates of all $H_{\boldsymbol{k}}$. In the HK model with Chern bands defined in Eq. (42), we have two energy bands per spin ($N_\alpha = 2$), and the Hilbert space dimension of each $H_{\boldsymbol{k}}$ is $\dim = 2^{2N_\alpha} = 16$. Among these states, $N_{\boldsymbol{k}} = 0, 4$ has $\binom{4}{0} = \binom{4}{4} = 1$ eigenstate, $N_{\boldsymbol{k}} = 1, 3$ has $\binom{4}{1} = \binom{4}{3} = 4$ eigenstates, and $N_{\boldsymbol{k}} = 2$ has $\binom{4}{2} = 6$ eigenstates.

Due to the SU(2) spin rotation symmetry, the $6 \times 6$ Hamiltonian $H_{\boldsymbol{k}}$ in the $N_{\boldsymbol{k}} = 2$ sector can be reduced to a block-diagonal form. Among these diagonal blocks, the largest is $3 \times 3$, which contains three SU(2) singlet states. This means the analytic results of many-body wave functions, Green's functions, and susceptibilities can only be expressed by cubic roots, which will be highly complicated and not be able to offer substantial insights. In contrast to the complicated analytic expressions involved in obtaining many-body wave functions, the Hamiltonian $H_{\boldsymbol{k}} - \mu N_{\boldsymbol{k}}$ is relatively straightforward to solve numerically since it is a $16 \times 16$ matrix for each $\boldsymbol{k}$. We denote these 16 states by $s = 1, 2, \ldots, 16$, whose energies increase with their indices $[E_{s=1}(\boldsymbol{k}) \leqslant E_{s=2}(\boldsymbol{k}) \leqslant \cdots \leqslant E_{s=16}(\boldsymbol{k})]$. We can also use a string of state indices $\{s_{\boldsymbol{k}}\}$ to represent a many-body wave function and energy:

$$|m\rangle = \bigotimes_{\boldsymbol{k}} \left|s^m_{\boldsymbol{k}}\right\rangle, \tag{B1}$$

$$E_m = \sum_{\boldsymbol{k}} E_{s^m_{\boldsymbol{k}}}(\boldsymbol{k}). \tag{B2}$$

Using these notations, the zero-temperature Green's function can be solved via the spectral decomposition as follows:

$$G_{\alpha\sigma,\beta\sigma'}(\boldsymbol{k}, z) = \frac{1}{D_{\boldsymbol{k}}} \sum_{s^g_{\boldsymbol{k}}=1}^{D_{\boldsymbol{k}}} \sum_{s^m_{\boldsymbol{k}}=1}^{16} \left( \frac{\left\langle s^g_{\boldsymbol{k}}\right| c_{\boldsymbol{k}\alpha\sigma} \left|s^m_{\boldsymbol{k}}\right\rangle \left\langle s^m_{\boldsymbol{k}}\right| c^\dagger_{\boldsymbol{k}\beta\sigma'} \left|s^g_{\boldsymbol{k}}\right\rangle}{z + E_{s^g_{\boldsymbol{k}}}(\boldsymbol{k}) - E_{s^m_{\boldsymbol{k}}}(\boldsymbol{k})} - \frac{\left\langle s^g_{\boldsymbol{k}}\right| c^\dagger_{\boldsymbol{k}\beta\sigma'} \left|s^m_{\boldsymbol{k}}\right\rangle \left\langle s^m_{\boldsymbol{k}}\right| c_{\boldsymbol{k}\alpha\sigma} \left|s^g_{\boldsymbol{k}}\right\rangle}{z - E_{s^g_{\boldsymbol{k}}}(\boldsymbol{k}) + E_{s^m_{\boldsymbol{k}}}(\boldsymbol{k})} \right), \tag{B3}$$

in which $D_{\boldsymbol{k}}$ stands for the ground-state degeneracy of the Hamiltonian $H_{\boldsymbol{k}}$. Figure 3(b) in the main text is numerically computed with Eq. (B3).

Similarly, the charge-current susceptibility can also be written as a spectral decomposition:

$$\chi_{0j}(\boldsymbol{q}, i\Omega) = \prod_{\boldsymbol{k}'} \frac{1}{D_{\boldsymbol{k}'}} \sum_{g\in\mathcal{G}} \sum_{m} \left( \frac{\langle g|\rho_{\boldsymbol{q}}|m\rangle \langle m|J^j_{-\boldsymbol{q}}|g\rangle}{i\Omega + E_g - E_m} - \frac{\langle g|J^j_{-\boldsymbol{q}}|m\rangle \langle m|\rho_{\boldsymbol{q}}|g\rangle}{i\Omega - E_g + E_m} \right). \tag{B4}$$

We first study the basic features of the numerator appearing in the spectral decomposition. Both $J^j_{-\boldsymbol{q}}$ and $\rho_{\boldsymbol{q}}$ operators contain $c, c^\dagger$ operators from the whole Brillouin zone, thus they have to be treated with caution. For generic many-body eigenstates $|g\rangle$ and $|m\rangle$, the matrix elements appearing in the spectral decomposition have the following form:

$$\langle g|\rho_{\boldsymbol{q}}|m\rangle \langle m|J^j_{-\boldsymbol{q}}|g\rangle = \frac{1}{N_L} \sum_{\boldsymbol{k}_1,\boldsymbol{k}_2} \langle g| \sum_{\alpha\sigma} c^\dagger_{\boldsymbol{k}_1+\frac{\boldsymbol{q}}{2}\alpha\sigma} c_{\boldsymbol{k}_1-\frac{\boldsymbol{q}}{2}\alpha\sigma} |m\rangle \langle m| \sum_{\alpha'\sigma'\beta\sigma''} v^j_{\alpha'\sigma',\beta,\sigma''}(\boldsymbol{k}_2) c^\dagger_{\boldsymbol{k}_2-\frac{\boldsymbol{q}}{2}\alpha'\sigma'} c_{\boldsymbol{k}_2+\frac{\boldsymbol{q}}{2}\beta\sigma''} |g\rangle. \tag{B5}$$

Now we analyze the condition of obtaining a nonzero element. The matrix element $\langle m|c^\dagger_{\boldsymbol{k}_2-\frac{\boldsymbol{q}}{2}\alpha'\sigma'} c_{\boldsymbol{k}_2+\frac{\boldsymbol{q}}{2}\beta\sigma''}|g\rangle$ in the above equation indicates that the state $|m\rangle$ must have *one more* electron at $\boldsymbol{k}_2 - \frac{\boldsymbol{q}}{2}$ and *one less* electron at $\boldsymbol{k}_2 + \frac{\boldsymbol{q}}{2}$ than the state $|g\rangle$. At any other momentum $\boldsymbol{k}' \neq \boldsymbol{k} \pm \frac{\boldsymbol{q}}{2}$, the state $s^m_{\boldsymbol{k}'}$ has to be identical to $s^g_{\boldsymbol{k}'}$. Otherwise, the matrix element will simply be zero. For the same reason, the matrix element $\langle g|c^\dagger_{\boldsymbol{k}_1+\frac{\boldsymbol{q}}{2}\alpha\sigma} c_{\boldsymbol{k}_1-\frac{\boldsymbol{q}}{2}\alpha\sigma}|m\rangle$ being nonzero implies that the same $|m\rangle$ state has *one more* electron at $\boldsymbol{k}_1 - \frac{\boldsymbol{q}}{2}$, and *one less* electron at $\boldsymbol{k}_1 + \frac{\boldsymbol{q}}{2}$ than the state $|g\rangle$ when the element is nonzero. Therefore, only the terms with $\boldsymbol{k}_1 = \boldsymbol{k}_2$ will contribute to the susceptibility spectral decomposition. This is a direct consequence of electron number conservation for each $\boldsymbol{k}$.

Now we write the states $|g\rangle$ and $|m\rangle$ as the products of eigenstates of $H_{\boldsymbol{k}}$, and the matrix elements will become

$$\langle g|\rho_{\boldsymbol{q}}|m\rangle \langle m|J^j_{-\boldsymbol{q}}|g\rangle = \frac{1}{N_L} \sum_{\boldsymbol{k}} \prod_{\boldsymbol{k}'\neq\boldsymbol{k}\pm\frac{\boldsymbol{q}}{2}} \delta_{s^g_{\boldsymbol{k}'},s^m_{\boldsymbol{k}'}} \left\langle s^g_{\boldsymbol{k}+\frac{\boldsymbol{q}}{2}}, s^g_{\boldsymbol{k}-\frac{\boldsymbol{q}}{2}}\right| \rho_{\boldsymbol{q},\boldsymbol{k}} \left|s^m_{\boldsymbol{k}+\frac{\boldsymbol{q}}{2}}, s^m_{\boldsymbol{k}-\frac{\boldsymbol{q}}{2}}\right\rangle \left\langle s^m_{\boldsymbol{k}+\frac{\boldsymbol{q}}{2}}, s^m_{\boldsymbol{k}-\frac{\boldsymbol{q}}{2}}\right| J^j_{-\boldsymbol{q},\boldsymbol{k}} \left|s^g_{\boldsymbol{k}+\frac{\boldsymbol{q}}{2}}, s^g_{\boldsymbol{k}-\frac{\boldsymbol{q}}{2}}\right\rangle, \tag{B6}$$

in which the operators $\rho_{\boldsymbol{q},\boldsymbol{k}}$ and $J^j_{\boldsymbol{q},\boldsymbol{k}}$ are defined as

$$\rho_{\boldsymbol{q},\boldsymbol{k}} = \sum_{\alpha\sigma} c^\dagger_{\boldsymbol{k}+\frac{\boldsymbol{q}}{2}\alpha\sigma} c_{\boldsymbol{k}-\frac{\boldsymbol{q}}{2}\alpha\sigma}, \tag{B7}$$

$$J^{j}_{\boldsymbol{q},\boldsymbol{k}} = \sum_{\alpha\sigma,\beta\sigma'} v^{j}_{\alpha\sigma,\beta\sigma'}(\boldsymbol{k}) c^{\dagger}_{\boldsymbol{k}+\frac{\boldsymbol{q}}{2}\alpha\sigma} c_{\boldsymbol{k}-\frac{\boldsymbol{q}}{2}\beta\sigma'}. \tag{B8}$$

For each term evolving fermion operators from $\boldsymbol{k} \pm \frac{\boldsymbol{q}}{2}$, there will also be $\prod_{k' \neq k \pm q/2} D_{k'}$ degenerate ground states that contribute identically to the current correlation function. Therefore, by combining Eqs. (B4) and (B6), the susceptibility can eventually be reorganized into the following form:

$$\chi_{0j}(\boldsymbol{q}, i\Omega) = \frac{1}{N_L} \sum_{\boldsymbol{k}} \frac{1}{D_{\boldsymbol{k}+\frac{\boldsymbol{q}}{2}} D_{\boldsymbol{k}-\frac{\boldsymbol{q}}{2}}} \sum_{s^{g}_{\boldsymbol{k}+\frac{\boldsymbol{q}}{2}}=1}^{D_{\boldsymbol{k}+\frac{\boldsymbol{q}}{2}}} \sum_{s^{g}_{\boldsymbol{k}-\frac{\boldsymbol{q}}{2}}=1}^{D_{\boldsymbol{k}-\frac{\boldsymbol{q}}{2}}} \sum_{s^{m}_{\boldsymbol{k}\pm\frac{\boldsymbol{q}}{2}}=1}^{16} \left( \frac{\left\langle s^{g}_{\boldsymbol{k}+\frac{\boldsymbol{q}}{2}}, s^{g}_{\boldsymbol{k}-\frac{\boldsymbol{q}}{2}} \middle| \rho_{\boldsymbol{q},\boldsymbol{k}} \middle| s^{m}_{\boldsymbol{k}+\frac{\boldsymbol{q}}{2}}, s^{m}_{\boldsymbol{k}-\frac{\boldsymbol{q}}{2}} \right\rangle \left\langle s^{m}_{\boldsymbol{k}+\frac{\boldsymbol{q}}{2}}, s^{m}_{\boldsymbol{k}-\frac{\boldsymbol{q}}{2}} \middle| J^{j}_{-\boldsymbol{q},\boldsymbol{k}} \middle| s^{g}_{\boldsymbol{k}+\frac{\boldsymbol{q}}{2}}, s^{g}_{\boldsymbol{k}-\frac{\boldsymbol{q}}{2}} \right\rangle}{i\Omega + E_{s^{g}_{\boldsymbol{k}+\frac{\boldsymbol{q}}{2}}}\left(\boldsymbol{k}+\frac{\boldsymbol{q}}{2}\right) + E_{s^{g}_{\boldsymbol{k}-\frac{\boldsymbol{q}}{2}}}\left(\boldsymbol{k}-\frac{\boldsymbol{q}}{2}\right) - E_{s^{m}_{\boldsymbol{k}+\frac{\boldsymbol{q}}{2}}}\left(\boldsymbol{k}+\frac{\boldsymbol{q}}{2}\right) - E_{s^{m}_{\boldsymbol{k}-\frac{\boldsymbol{q}}{2}}}\left(\boldsymbol{k}-\frac{\boldsymbol{q}}{2}\right)} \right.$$

$$\left. - \frac{\left\langle s^{g}_{\boldsymbol{k}+\frac{\boldsymbol{q}}{2}}, s^{g}_{\boldsymbol{k}-\frac{\boldsymbol{q}}{2}} \middle| J^{j}_{-\boldsymbol{q},\boldsymbol{k}} \middle| s^{m}_{\boldsymbol{k}+\frac{\boldsymbol{q}}{2}}, s^{m}_{\boldsymbol{k}-\frac{\boldsymbol{q}}{2}} \right\rangle \left\langle s^{m}_{\boldsymbol{k}+\frac{\boldsymbol{q}}{2}}, s^{m}_{\boldsymbol{k}-\frac{\boldsymbol{q}}{2}} \middle| \rho_{\boldsymbol{q},\boldsymbol{k}} \middle| s^{g}_{\boldsymbol{k}+\frac{\boldsymbol{q}}{2}}, s^{g}_{\boldsymbol{k}-\frac{\boldsymbol{q}}{2}} \right\rangle}{i\Omega - E_{s^{g}_{\boldsymbol{k}+\frac{\boldsymbol{q}}{2}}}\left(\boldsymbol{k}+\frac{\boldsymbol{q}}{2}\right) - E_{s^{g}_{\boldsymbol{k}-\frac{\boldsymbol{q}}{2}}}\left(\boldsymbol{k}-\frac{\boldsymbol{q}}{2}\right) + E_{s^{m}_{\boldsymbol{k}+\frac{\boldsymbol{q}}{2}}}\left(\boldsymbol{k}+\frac{\boldsymbol{q}}{2}\right) + E_{s^{m}_{\boldsymbol{k}-\frac{\boldsymbol{q}}{2}}}\left(\boldsymbol{k}-\frac{\boldsymbol{q}}{2}\right)} \right). \tag{B9}$$

This susceptibility can also be numerically evaluated using the eigenstates of the many-body Hamiltonian $H_{\boldsymbol{k}}$ for each $\boldsymbol{k}$. The results shown in Figs. 3(c) and 3(d) are obtained using Eq. (B9).


[1] N. P. Armitage, E. J. Mele, and A. Vishwanath, Weyl and Dirac semimetals in three-dimensional solids, Rev. Mod. Phys. **90**, 015001 (2018).

[2] N. Nagaosa, T. Morimoto, and Y. Tokura, Transport, magnetic and optical properties of Weyl materials, Nat. Rev. Mater. **5**, 621 (2020).

[3] B. Bradlyn, L. Elcoro, J. Cano, M. G. Vergniory, Z. Wang, C. Felser, M. I. Aroyo, and B. A. Bernevig, Topological quantum chemistry, Nature (London) **547**, 298 (2017).

[4] J. Cano, B. Bradlyn, Z. Wang, L. Elcoro, M. G. Vergniory, C. Felser, M. I. Aroyo, and B. A. Bernevig, Building blocks of topological quantum chemistry: Elementary band representations, Phys. Rev. B **97**, 035139 (2018).

[5] H. C. Po, A. Vishwanath, and H. Watanabe, Symmetry-based indicators of band topology in the 230 space groups, Nat. Commun. **8**, 50 (2017).

[6] H. Watanabe, H. C. Po, M. P. Zaletel, and A. Vishwanath, Filling-enforced gaplessness in band structures of the 230 space groups, Phys. Rev. Lett. **117**, 096404 (2016).

[7] J. Cano and B. Bradlyn, Band representations and topological quantum chemistry, Annu. Rev. Condens. Matter Phys. **12**, 225 (2021).

[8] M. Iraola, N. Heinsdorf, A. Tiwari, D. Lessnich, T. Mertz, F. Ferrari, M. H. Fischer, S. M. Winter, F. Pollmann, T. Neupert, R. Valentí, and M. G. Vergniory, Towards a topological quantum chemistry description of correlated systems: The case of the Hubbard diamond chain, Phys. Rev. B **104**, 195125 (2021).

[9] D. Lessnich, S. M. Winter, M. Iraola, M. G. Vergniory, and R. Valentí, Elementary band representations for the single-particle Green's function of interacting topological insulators, Phys. Rev. B **104**, 085116 (2021).

[10] M. O. Soldini, N. Astrakhantsev, M. Iraola, A. Tiwari, M. H. Fischer, R. Valentí, M. G. Vergniory, G. Wagner, and T. Neupert, Interacting topological quantum chemistry of Mott atomic limits, Phys. Rev. B **107**, 245145 (2023).

[11] Z. Wang and S.-C. Zhang, Simplified topological invariants for interacting insulators, Phys. Rev. X **2**, 031008 (2012).

[12] Z. Wang and B. Yan, Topological Hamiltonian as an exact tool for topological invariants, J. Phys.: Condens. Matter **25**, 155601 (2013).

[13] H. Hu, L. Chen, C. Setty, M. Garcia-Diez, S. E. Grefe, A. Prokofiev, S. Kirchner, M. G. Vergniory, S. Paschen, J. Cano, and Q. Si, Topological semimetals without quasiparticles electronic topology without free-electron counterpart, arXiv:2110.06182.

[14] H.-H. Lai, S. E. Grefe, S. Paschen, and Q. Si, Weyl-Kondo semimetal in heavy-fermion systems, Proc. Natl. Acad. Sci. USA **115**, 93 (2018).

[15] S. E. Grefe, H.-H. Lai, S. Paschen, and Q. Si, Weyl-Kondo semimetals in nonsymmorphic systems, Phys. Rev. B **101**, 075138 (2020).

[16] S. Dzsaber, L. Prochaska, A. Sidorenko, G. Eguchi, R. Svagera, M. Waas, A. Prokofiev, Q. Si, and S. Paschen, Kondo insulator to semimetal transformation tuned by spin-orbit coupling, Phys. Rev. Lett. **118**, 246601 (2017).

[17] S. Dzsaber, X. Yan, M. Taupin, G. Eguchi, A. Prokofiev, T. Shiroka, P. Blaha, O. Rubel, S. E. Grefe, H.-H. Lai, Q. Si, and S. Paschen, Giant spontaneous Hall effect in a nonmagnetic Weyl Kondo semimetal, Proc. Natl. Acad. Sci. USA **118**, e2013386118 (2021).

[18] L. Chen, C. Setty, H. Hu, M. G. Vergniory, S. E. Grefe, L. Fischer, X. Yan, G. Eguchi, A. Prokofiev, S. Paschen, J. Cano, and Q. Si, Topological semimetal driven by strong correlations and crystalline symmetry, Nat. Phys. **18**, 1341 (2022).

[19] C. Setty, S. Sur, L. Chen, F. Xie, H. Hu, S. Paschen, J. Cano, and Q. Si, Symmetry constraints and spectral crossing in a mott insulator with Green's function zeros, Phys. Rev. Res. **6**, L032018 (2024).

[20] I. Dzyaloshinskii, Some consequences of the Luttinger theorem: The luttinger surfaces in non-Fermi liquids and Mott insulators, Phys. Rev. B **68**, 085113 (2003).

[21] N. Wagner, L. Crippa, A. Amaricci, P. Hansmann, M. Klett, E. J. König, T. Schäfer, D. D. Sante, J. Cano, A. J. Millis *et al.*, Mott insulators with boundary zeros, Nat. Commun. **14**, 7531 (2023).

[22] A. A. Abrikosov, L. P. Gorkov, and I. E. Dzyaloshinski, *Methods of Quantum Field Theory in Statistical Physics* (Dover Publications Inc., New York, 2012).

[23] G. Kotliar, S. Y. Savrasov, K. Haule, V. S. Oudovenko, O. Parcollet, and C. A. Marianetti, Electronic structure calculations

with dynamical mean-field theory, Rev. Mod. Phys. **78**, 865 (2006).
[24] S. Florens and A. Georges, Slave-rotor mean-field theories of strongly correlated systems and the Mott transition in finite dimensions, Phys. Rev. B **70**, 035114 (2004).
[25] R. Yu and Q. Si, U (1) slave-spin theory and its application to Mott transition in a multiorbital model for iron pnictides, Phys. Rev. B **86**, 085104 (2012).
[26] S. Paschen and Q. Si, Quantum phases driven by strong correlations, Nat. Rev. Phys. **3**, 9 (2021).
[27] P. Fazekas, *Lecture Notes on Electron Correlation and Magnetism* (World Scientific, Singapore, 1999), Vol. 5.
[28] G. E. Volovik, *The Universe in a Helium Droplet* (Oxford University Press, Oxford, 2003), Vol. 117.
[29] A. Rosch, Breakdown of Luttinger's theorem in two-orbital Mott insulators, Eur. Phys. J. B **59**, 495 (2007).
[30] V. Gurarie, Single-particle Green's functions and interacting topological insulators, Phys. Rev. B **83**, 085426 (2011).
[31] A. M. Essin and V. Gurarie, Bulk-boundary correspondence of topological insulators from their respective Green's functions, Phys. Rev. B **84**, 125132 (2011).
[32] K. B. Dave, P. W. Phillips, and C. L. Kane, Absence of Luttinger's theorem due to zeros in the single-particle green function, Phys. Rev. Lett. **110**, 090403 (2013).
[33] K. Seki and S. Yunoki, Topological interpretation of the Luttinger theorem, Phys. Rev. B **96**, 085124 (2017).
[34] C. Setty, Pairing instability on a Luttinger surface: A non-Fermi liquid to superconductor transition and its Sachdev-Ye-Kitaev dual, Phys. Rev. B **101**, 184506 (2020).
[35] C. Setty, Superconductivity from luttinger surfaces: Emergent Sachdev-Ye-Kitaev physics with infinite-body interactions, Phys. Rev. B **103**, 014501 (2021).
[36] C. Setty, Dilute magnetic moments in an exactly solvable interacting host, arXiv:2105.15205.
[37] Y. Xu and C. Xu, Green's function zero and symmetric mass generation, arXiv:2103.15865.
[38] M. Fabrizio, Emergent quasiparticles at Luttinger surfaces, Nat. Commun. **13**, 1561 (2022).
[39] A. Blason and M. Fabrizio, Unified role of Green's function poles and zeros in topological insulators, Phys. Rev. B **108**, 125115 (2023).
[40] J. Zhao, P. Mai, B. Bradlyn, and P. Phillips, Failure of topological invariants in strongly correlated matter, Phys. Rev. Lett. **131**, 106601 (2023).
[41] Y.-Z. You, Y.-C. He, C. Xu, and A. Vishwanath, Symmetric fermion mass generation as deconfined quantum criticality, Phys. Rev. X **8**, 011026 (2018).
[42] D.-C. Lu, M. Zeng, J. Wang, and Y.-Z. You, Fermi surface symmetric mass generation, Phys. Rev. B **107**, 195133 (2023).
[43] D.-C. Lu, M. Zeng, and Y.-Z. You, Green's function zeros in Fermi surface symmetric mass generation, arXiv:2307.12223.
[44] K. Slagle, Y.-Z. You, and C. Xu, Exotic quantum phase transitions of strongly interacting topological insulators, Phys. Rev. B **91**, 115121 (2015).
[45] Y. Hatsugai and M. Kohmoto, Exactly solvable model of correlated lattice electrons in any dimensions, J. Phys. Soc. Jpn. **61**, 2056 (1992).
[46] D. J. Thouless, M. Kohmoto, M. P. Nightingale, and M. den Nijs, Quantized Hall conductance in a two-dimensional periodic potential, Phys. Rev. Lett. **49**, 405 (1982).
[47] Q. Niu, D. J. Thouless, and Y.-S. Wu, Quantized Hall conductance as a topological invariant, Phys. Rev. B **31**, 3372 (1985).
[48] P. W. Phillips, C. Setty, and S. Zhang, Absence of a charge diffusion pole at finite energies in an exactly solvable interacting flat-band model in d dimensions, Phys. Rev. B **97**, 195102 (2018).
[49] D. Manning-Coe and B. Bradlyn, Ground state stability, symmetry, and degeneracy in Mott insulators with long-range interactions, Phys. Rev. B **108**, 165136 (2023).
[50] G. Stefanucci and R. Van Leeuwen, *Nonequilibrium Many-body Theory of Quantum Systems: A Modern Introduction* (Cambridge University Press, New York, 2013).
[51] G. D. Mahan, *Many-particle Physics* (Springer Science+Business Media, New York, 2000).
[52] P. Coleman, *Introduction to Many-body Physics* (Cambridge University Press, Cambridge, 2015).
[53] P. Nozieres, *Theory of Interacting Fermi Systems* (CRC, Boca Raton, FL, 2018).
[54] O. Betbeder-Matibet and P. Nozières, Transport equation for quasiparticles in a system of interacting fermions colliding on dilute impurities, Ann. Phys. **37**, 17 (1966).
[55] L. P. Gavensky, S. Sachdev, and N. Goldman, Connecting the many-body Chern number to Luttinger's theorem through Středa's formula, Phys. Rev. Lett. **131**, 236601 (2023).
[56] J. M. Luttinger, Analytic properties of single-particle propagators for many-fermion systems, Phys. Rev. **121**, 942 (1961).